Endothelial Msx1 transduces hemodynamic changes into an arteriogenic remodeling response

Ine Vandersmissen,[1] Sander Craps,[1] Maarten Depypere,[2] Giulia Coppiello,[1,13] Nick van Gastel,[4,5] Frederik Maes,[2] Geert Carmeliet,[4,5] Jan Schrooten,[5,6] Elizabeth A.V. Jones,[1] Lieve Umans,[10,8] Roland Devlieger,[12,9] Michel Koole,[7] Olivier Gheysens,[11,7] An Zwijsen,[10,3] Xabier L. Aranguren,[1,13] and Aernout Luttun[1]

[1]Department of Cardiovascular Sciences, Center for Molecular and Vascular Biology; [2]Department of Electrical Engineering/Processing Speech and Images, Medical Image Computing; [3]Department of Human Genetics; [4]Laboratory of Clinical and Experimental Endocrinology, Division of Skeletal Tissue Engineering, Department of Clinical and Experimental Medicine; [5]Prometheus, Division of Skeletal Tissue Engineering; [6]Department of Materials Engineering; [7]Department of Imaging and Pathology; [8]Laboratory of Molecular Biology (Celgen), Department of Development and Regeneration; [9]Department of Development and Regeneration; and [10]Laboratory of Developmental Signaling, VIB Center for the Biology of Disease, KU Leuven, 3000 Leuven, Belgium
[11]Department of Nuclear Medicine and [12]Department of Gynecology and Obstetrics, University Hospital Leuven, 3000 Leuven, Belgium
[13]Hematology and Cell Therapy Area, Clínica Universidad de Navarra and Division of Oncology, Center for Applied Medical Research, University of Navarra, 31008 Pamplona, Spain

Collateral remodeling is critical for blood flow restoration in peripheral arterial disease and is triggered by increasing fluid shear stress in preexisting collateral arteries. So far, no arterial-specific mediators of this mechanotransduction response have been identified. We show that muscle segment homeobox 1 (MSX1) acts exclusively in collateral arterial endothelium to transduce the extrinsic shear stimulus into an arteriogenic remodeling response. MSX1 was specifically up-regulated in remodeling collateral arteries. MSX1 induction in collateral endothelial cells (ECs) was shear stress driven and downstream of canonical bone morphogenetic protein–SMAD signaling. Flow recovery and collateral remodeling were significantly blunted in EC-specific *Msx1/2* knockout mice. Mechanistically, MSX1 linked the arterial shear stimulus to arteriogenic remodeling by activating the endothelial but not medial layer to a proinflammatory state because EC but not smooth muscle cell*Msx1/2* knockout mice had reduced leukocyte recruitment to remodeling collateral arteries. This reduced leukocyte infiltration in EC *Msx1/2* knockout mice originated from decreased levels of intercellular adhesion molecule 1 (ICAM1)/vascular cell adhesion molecule 1 (VCAM1), whose expression was also in vitro driven by promoter binding of MSX1.

Introduction

The vasculature delivers nutrients and oxygen throughout the body. As a result of the high diversity of functions and environmental signals in each vascular bed, endothelial cells (ECs) forming the inner layer of the vasculature adapt themselves to their context-dependent needs. This results in a high degree of EC heterogeneity. For large conduit vessels, there are major molecular, structural, and functional differences between arterial and venous ECs (Aird, 2007). Acquisition of these differences is not only intrinsically predetermined by genetic factors early during development, but is also influenced by extrinsic cues from the changing environment (dela Paz and D'Amore, 2009). We and others illustrated this EC plasticity by the dramatic loss of arterial- and venous-specific fingerprints when ECs become deprived of environmental signals in cell culture (Amatschek et al., 2007; Aranguren et al., 2013). For arterial ECs, their specific characteristics can be partly restored in vitro by exposing them to an arterial flow pattern (Obi et al., 2009; Buschmann et al., 2010). The dependence of arterial identity on its hemodynamic environment was also shown in vivo in chick (Moyon et al., 2001; le Noble et al., 2004; Buschmann et al., 2010) and mouse (Jones et al., 2008) embryos.

EC adaptation to the environment not only occurs during development but also in pathological conditions such as peripheral arterial disease (PAD). PAD affected >200 million patients worldwide in 2010 and became the third leading cause of atherosclerotic cardiovascular morbidity (Fowkes et al., 2013). Because patient numbers continuously increase, we are in critical need of efficient therapies designed on the basis of the molecular understanding of the adaptive vascular response (Annex,

Correspondence to Aernout Luttun: aernout.luttun@med.kuleuven.be

Abbreviations used in this paper: ALK, activin receptor-like kinase; αSMA, smooth muscle α-actin; BMP, bone morphogenetic protein; ChIP, chromatin immunoprecipitation; DMH1, dorsomorphin homologue 1; EC, endothelial cell; ENG, endoglin; HIAEC, human iliac artery EC; HUAEC, human umbilical cord artery EC; HUVEC, human umbilical cord vein EC; ICAM1, intercellular adhesion molecule 1; IF, immunofluorescence; KLF2, Kruppel-like factor 2; LSS, laminar shear stress; micro-CT, microcomputed tomography; MSX, muscle segment homeobox; PAD, peripheral arterial disease; PET, positron emission tomography; qRT-PCR, quantitative RT-PCR; SMC, smooth muscle cell; TF, transcription factor; VCAM1, vascular cell adhesion molecule 1; VOI, volume of interest.

The Rockefeller University Press $30.00
J. Cell Biol. Vol. 210 No. 7 1239–1256
www.jcb.org/cgi/doi/10.1083/jcb.201502003

2013). The clinical outcome of an occlusion is largely determined by the extent of the preexisting collateral arterial network and its capacity to remodel into a fully functional arterial bypass circuit (Meier et al., 2007; Chalothorn and Faber, 2010), a process known as adaptive arteriogenesis (Scholz et al., 2002). The obstruction of a large artery increases the pressure difference over the preexisting collateral arteries that connect the nonperfused tissue distal to the occlusion site with a perfused vascular network. This yields an increased blood flow through interconnecting collaterals. The concomitant raised laminar shear stress (LSS) is the driving stimulus of arteriogenic remodeling (Eitenmüller et al., 2006) and activates ECs, triggering the attraction of monocytes through secretion of monocyte chemoattractant protein 1 (Ito et al., 1997) and increased expression of adhesion molecules such as intercellular adhesion molecule 1 (ICAM1) and vascular cell adhesion molecule 1 (VCAM1; Scholz et al., 2000; Pipp et al., 2004). Subsequently, these monocytes mature into macrophages and support the outward collateral remodeling process predominantly through a paracrine effect on the medial cell layer (Arras et al., 1998). Although this process is specific for the arterial vascular bed, so far no arterial-specific factor has been identified that mediates the transcriptional transduction of the extrinsic arterial shear stimulus into the inflammation-driven arteriogenic remodeling response.

To identify regulators of vascular bed–specific characteristics of ECs, we recently established an arteriovenous fingerprint of freshly isolated, uncultured human ECs, which retain both their intrinsically and extrinsically determined expression pattern (Aranguren et al., 2013). As part of this fingerprint, eight arterially enriched transcription factors (TFs) were identified, including muscle segment homeobox 1 (MSX1), a downstream effector of the bone morphogenetic protein (BMP) pathway. A genetic study demonstrated that inadequate BMP signaling causes vascular diseases such as pulmonary arterial hypertension and hereditary hemorrhagic telangiectasia (Cai et al., 2012). Current studies on BMP signaling in the arterial vascular bed have mainly focused on the ligand/receptor level of this pathway (Urness et al., 2000; Seki et al., 2003; Sorensen et al., 2003; Mancini et al., 2009; Seghers et al., 2012; Somekawa et al., 2012). Only recently have the first studies been published describing that extrinsic hemodynamic changes activate SMAD1/5/8 proteins, the intracellular mediators of canonical BMP signaling (Zhou et al., 2012, 2013), but no downstream TFs have been identified so far. Although arterial-specific endothelial expression of MSX1 has been reported in mice, neither its functional role in the endothelium nor the underlying mechanism for its arterial-specific expression have been established (Lopes et al., 2011, 2012). Here, we demonstrate that exterior arterial shear stress induces expression of the arterial-specific TF MSX1, resulting in an inflammation-driven arteriogenic remodeling response in ischemic hind limbs of mice subjected to PAD.

Results

MSX1 is an arterial-specific TF reexpressed during pathological remodeling

The *Msx* family in mice consists of *Msx1*, *Msx2*, and *Msx3*, of which only the former two are preserved in humans (Finnerty et al., 2009). By assessing MSX expression in freshly isolated ECs from human umbilical cord samples by microarray and by staining cross sections of this tissue (Aranguren et al., 2013), we found MSX1 to be specifically localized in the arterial endothelium, whereas MSX2 was equally present in arterial and venous ECs (Fig. S1). Immunofluorescence (IF) staining demonstrated that the asymmetric localization for MSX1 was also present in the developing mouse embryo, whereas its expression was largely lost in adult quiescent endothelium (unpublished data), in agreement with previous studies (Goupille et al., 2008; Lopes et al., 2012).

In pathological conditions, ECs become reactivated and reexpress part of their developmental gene signature in response to their changing environment (Buschmann et al., 2010). Therefore, we evaluated MSX1 expression during arterial remodeling in a mouse PAD model. Hind limb ischemia was induced by occluding the right femoral artery. MSX expression was analyzed in transversal sections of the adductor region 7 d later, a stage when the collateral remodeling response is most prominent (Herzog et al., 2002). MSX1 expression was strongly induced in the intimal, medial, and adventitial layers of collateral arteries within the right adductor region, whereas MSX2 was only induced in the adventitial layer compared with the contralateral nonligated side (Fig. 1, A and B). Within the endothelium, MSX1 was specifically induced in arterial ECs lining preexisting collateral arteries and not expressed nor induced in venous ECs, whereas MSX2 maintained a baseline expression level both in arterial and venous ECs (Fig. 1, C–F). These data demonstrate that MSX1, unlike MSX2, is an arterial-specific TF highly induced during the arteriogenic remodeling process.

LSS but not hypoxia induces MSX1 expression in ECs

After an arterial occlusion, blood flow is redirected through preexisting collaterals, which generates a sudden increase in shear stress on the endothelium. To assess whether reexpression of MSX1 in collateral endothelium is dependent on this hemodynamic cue, early passage human umbilical cord artery ECs (HUAECs) were exposed to a sudden increase in LSS. Their response to flow was evident from their alignment in the flow direction and increased expression of *Kruppel-like factor 2* (*KLF2*; Fig. S2, A and B; Dekker et al., 2002). *MSX1* increased upon LSS exposure as measured by quantitative RT-PCR (qRT-PCR) both in HUAECs and human iliac artery ECs (HIAECs; Fig. 2 A and Fig. S2, C and D). Flow-triggered MSX1 induction in HUAECs was confirmed at the protein level by Western blot and IF (Fig. 2, B and C; and Fig. S2 E). Unlike LSS, hypoxia, the main driver of sprouting angiogenesis, did not trigger endothelial *MSX1* expression, whereas the hypoxia-sensitive *VEGF* was induced under such conditions (Fig. S2 F). This response pattern of MSX1 is compatible with a primary role of shear-driven arteriogenic remodeling in the normoxic adductor to restore blood supply after an occlusion (Scholz et al., 2002).

LSS-dependent canonical BMP signaling triggers MSX1 expression in ECs

To gain insight into the molecular mechanisms underlying flow-induced MSX1 expression, we examined the role of BMP pathway components in our in vitro model. First, we focused on SMAD1/5/8 proteins, the intracellular mediators of canonical BMP signaling, and found enriched phosphorylation and hence activation of SMAD1/5/8 upon LSS exposure (Fig. 2, B and C; and Fig. S2 E), in agreement with previous studies on increased pSMAD1/5/8 in changing hemodynamic conditions (Zhou et al., 2012, 2013). Moreover, siRNA-mediated knockdown of

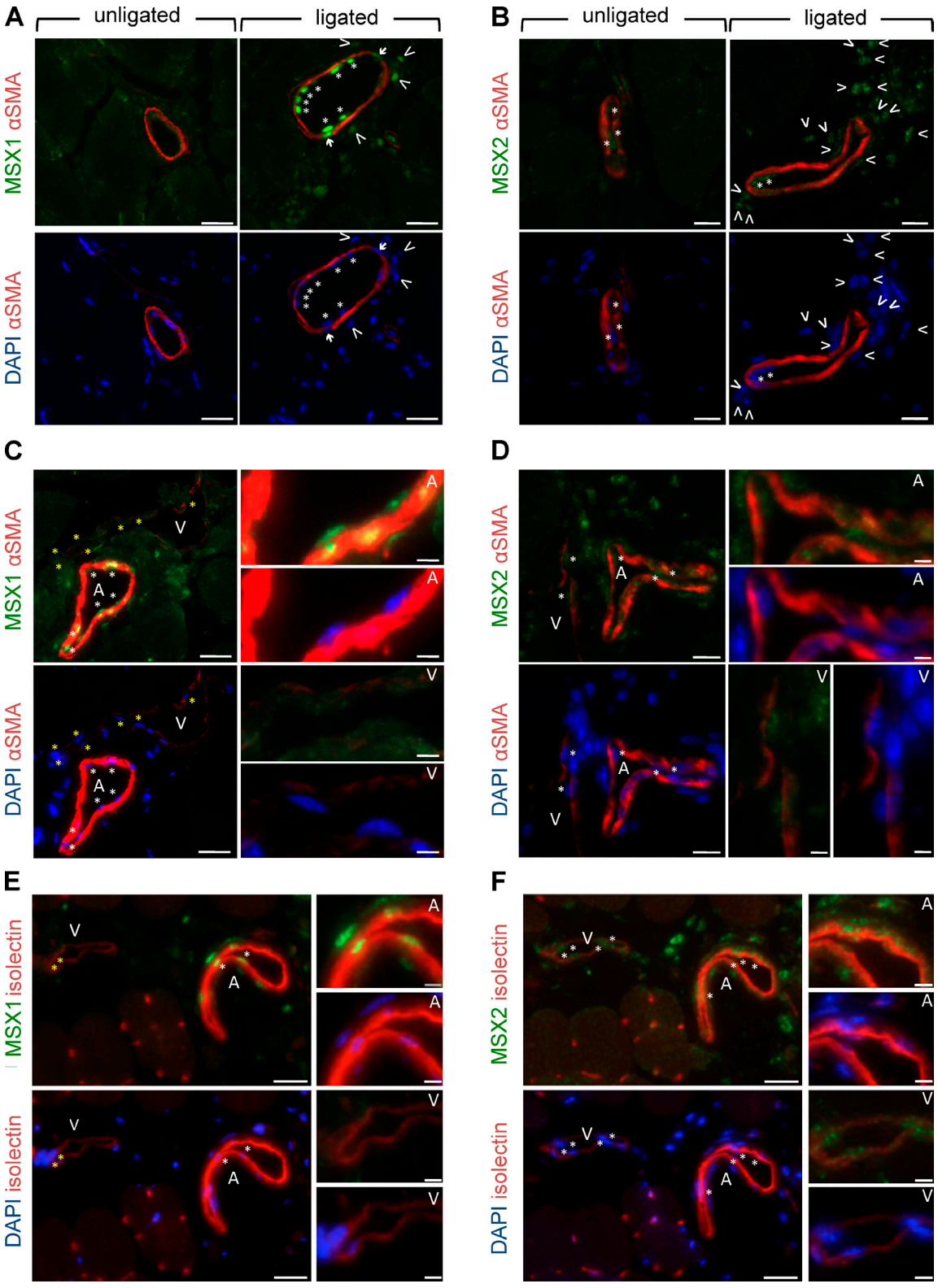

Figure 1. **MSX1 is an arterial-specific TF reexpressed during arteriogenic remodeling.** (A and B) IF staining for MSX1 or MSX2 (green) and αSMA (red) in unligated (left) and 7-d ligated (right) adductors. DAPI (in blue) was used as a nuclear counterstain with asterisks, arrows, and arrowheads indicating positive ECs, SMCs, and adventitial cells, respectively. (C and D) IF staining for MSX1 or MSX2 (green), αSMA (red), and DAPI (blue) in the right adductor 7 d after femoral artery ligation. (E and F) IF staining for MSX1 or MSX2 (green), isolectin GS-IB_4 (red), and DAPI (blue) on sequential sections in the adductor 7 d after femoral artery ligation. (C–F) The white and yellow asterisks indicate positive and negative ECs, respectively. A, artery; V, vein. Bars: (A and C) 25 µm; (B and D) 15 µm; (E and F) 20 µm; (magnifications in C and D) 5 µm; (magnifications in E and F) 20 µm.

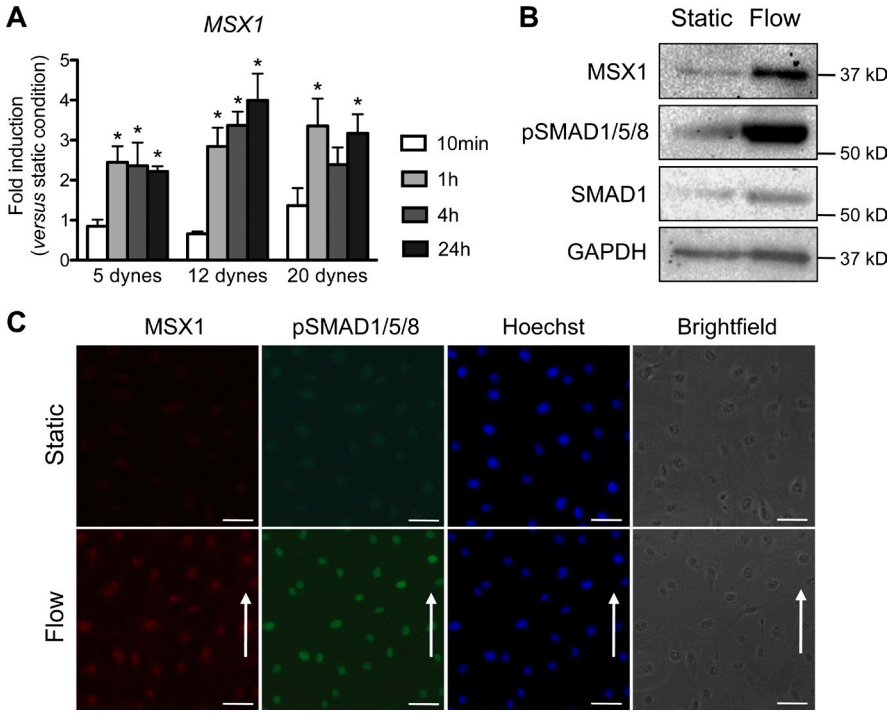

Figure 2. **Endothelial MSX1 expression is induced by a changing hemodynamic environment.** (A) Expression analysis by qRT-PCR of HUAECs seeded on fibronectin-coated chambers kept in static conditions or exposed to different LSS levels over time. *MSX1* mRNA expression is represented relative to the static condition. $n = 3$ for 5 dynes and $n = 8$ for 12 and 20 dynes. Error bars represent the SEM. *, $P < 0.05$ versus static condition. (B) Western blot of total cell lysates of HUAECs kept in static conditions or exposed to LSS of 20 dynes/cm^2 for 1 h for MSX1, pSMAD1/5/8, SMAD1, and GAPDH. (C) IF staining on HUAECs with and without exposure to LSS of 20 dynes/cm^2 for 1 h for MSX1 (red), phosphorylated (p)SMAD1/5/8 (green), and Hoechst (nuclear marker in blue) and the corresponding brightfield pictures. The arrows represent the flow direction. Bars, 50 µm.

SMAD1 and *SMAD5* showed that canonical BMP signaling is indispensable for the induction of MSX1 upon LSS exposure both on the RNA and protein level (Fig. 3, A and B; and Fig. S3, A–C). Phosphorylation of the SMAD1/5/8 proteins occurs upon activation of a heteromeric complex of type I and II receptors (type I, activin receptor-like kinase [ALK] 1, 2, 3, or 6 and type II, activin receptor type IIA or IIB or BMP type II receptor [BMPR2]) and can be potentiated by type III coreceptors such as Endoglin (ENG; Cai et al., 2012). To identify the receptors involved, we performed shear stress experiments in the presence or absence of dorsomorphin homologue 1 (DMH1), a specific inhibitor of the type I receptors ALK1/2/3 (Hao et al., 2010; Cross et al., 2011) and found that *MSX1* induction upon LSS exposure was still present upon DMH1 treatment (Fig. 3 C). On the other hand, siRNA-mediated silencing of *ALK6*, another BMP type I receptor, or the type II receptor *BMPR2* did abrogate LSS-induced *MSX1* up-regulation (Fig. 3, D and E). Finally, because ENG is the only component of the BMP pathway that has been previously shown to have a functional role in collateral remodeling (Seghers et al., 2012), we hypothesized a potential mechanistic role for ENG in the shear-driven BMP signaling cascade. Knockdown of *ENG* expression attenuated flow-induced *MSX1* induction (Fig. 3 F). The onset of flow was confirmed by the assessment of *KLF2* induction versus the static control in each condition, and knockdown efficiency was validated in all experiments (Fig. S3, D–I). All together, we demonstrate that the ALK6/BMPR2/ENG–SMAD1/5/8 signaling cascade is indispensable for LSS-driven up-regulation of *MSX1* in arterial ECs.

Paracrine BMP2/6 signaling triggers MSX1 expression in smooth muscle cells (SMCs)

In addition to ECs, MSX1 expression was also induced in SMCs (Fig. 1 A). Shear stress only acts on the EC lining and hence cannot be directly responsible for MSX1 induction in the SMC layer of remodeling collateral arteries. Because, during changing hemodynamic conditions, activated canonical BMP signaling in the medial, but not the EC, layer is dependent on BMP2/4/6 ligands (Zhou et al., 2012), we hypothesized that MSX1 induction in SMCs under changing hemodynamic conditions could occur downstream of BMP2/4/6 signaling through paracrine cross talk with shear-activated ECs. We found that LSS-exposed ECs specifically and significantly increased their *BMP2* and *BMP6* expression (Fig. 3 G). Although exposure to BMP2 or BMP6 induced *MSX1* expression in SMCs, ECs did not have this response, suggesting that LSS-induced endothelial BMP2/6 production could trigger *MSX1* expression in neighboring SMCs, but not in an autocrine loop (Fig. 3 H).

BMP signaling is required for flow-triggered endothelial Msx1 expression during arteriogenesis in vivo

Next, we tested whether SMAD-mediated signaling is responsible for MSX1 induction during flow-driven collateral remodeling in vivo. Increased SMAD1/5/8 activity was present in the three vascular layers of collateral arteries 7 d after ligation (Fig. 4 A), reminiscent of the induction pattern of MSX1 (Fig. 1 A). In unligated adductors, a ubiquitous pSMAD1/5/8 baseline activity was found throughout the arterial and venous endothelium, like in the developing mouse embryo (Moya et al., 2012). Upon arterial occlusion, SMAD1/5/8 activity became specifically enriched within arterial ECs of the remodeling collaterals (Fig. S4 A). Next, we examined colocalization for components of different levels of the BMP pathway and found a colocalization within the collateral ECs for ENG and pSMAD1/5/8 on the one hand and pSMAD1/5/8 and MSX1 on the other hand (Fig. 4, B and C). The analysis of MSX1 and pSMAD1/5/8 confirmed the induction of both MSX1 and pSMAD1/5/8 in arterial collateral endothelium (Fig. 4 C). These data complement our in vitro results and support that BMP–SMAD signaling also regulates MSX1 during adaptive arteriogenesis in vivo.

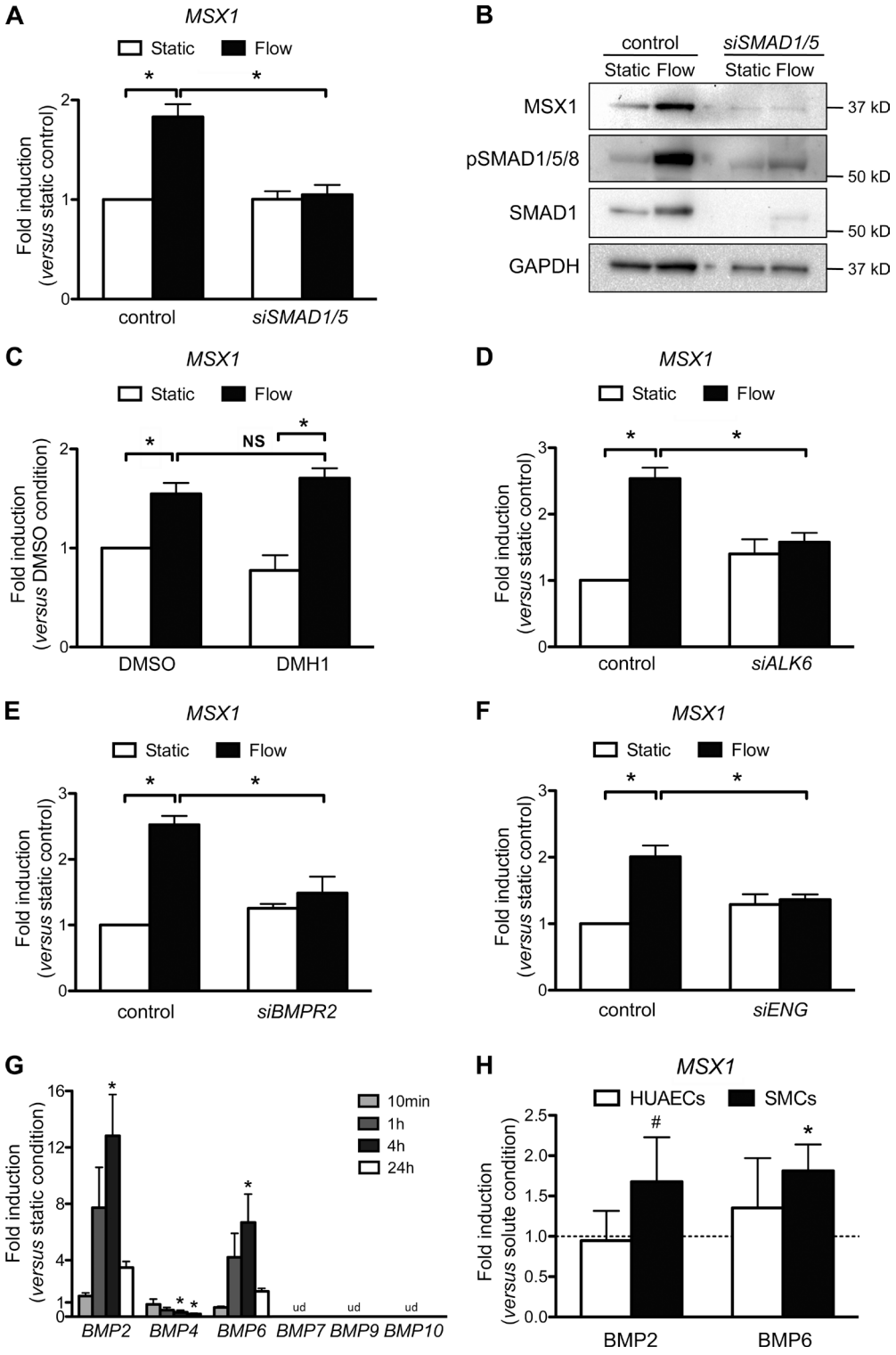

Figure 3. **LSS-dependent canonical BMP signaling triggers MSX1 expression in ECs.** (A) HUAECs were transfected with control siRNA or siRNA against *SMAD1/5*, seeded in fibronectin-coated chambers, and subsequently kept static or subjected for 1 h to an LSS of 20 dynes/cm^2. *MSX1* expression was analyzed and represented relative to the control static condition. $n = 7$. (B) Corresponding representative Western blot analysis for MSX1, pSMAD1/5/8, SMAD1, and GAPDH. (C) HUAECs were pretreated for 1 h with DMSO or 2.5-µM DMH1 and subjected to static or LSS (20 dynes/cm^2) conditions for 1 h in the presence of DMSO or DMH1. *MSX1* expression was analyzed and represented relative to the DMSO condition. $n = 3$. (D–F) Cells transfected with control siRNA or siRNA against *ALK6* ($n = 5$), *BMPR2* ($n = 6$), or *ENG* ($n = 4$) were exposed to static or flow conditions and were analyzed for *MSX1* expression. *, $P < 0.05$ versus the indicated condition. (G) qRT-PCR analysis of HUAECs kept in static conditions or exposed to LSS (20 dynes/cm^2 for the indicated times). mRNA expression is represented relative to the static condition. $n = 3$. (A, C, and D–F) *, $P < 0.05$ versus static condition. ud, undetectable. (H) qRT-PCR analysis of HUAECs and SMCs serum starved for 1 h and exposed to 10 ng/µl BMP2, BMP6, or the corresponding amount of solute for 48 h. mRNA expression is represented relative to the control condition. $n = 4$ and 7. *, $P < 0.05$; #, $P = 0.13$ versus corresponding solute condition. Error bars represent the SEM.

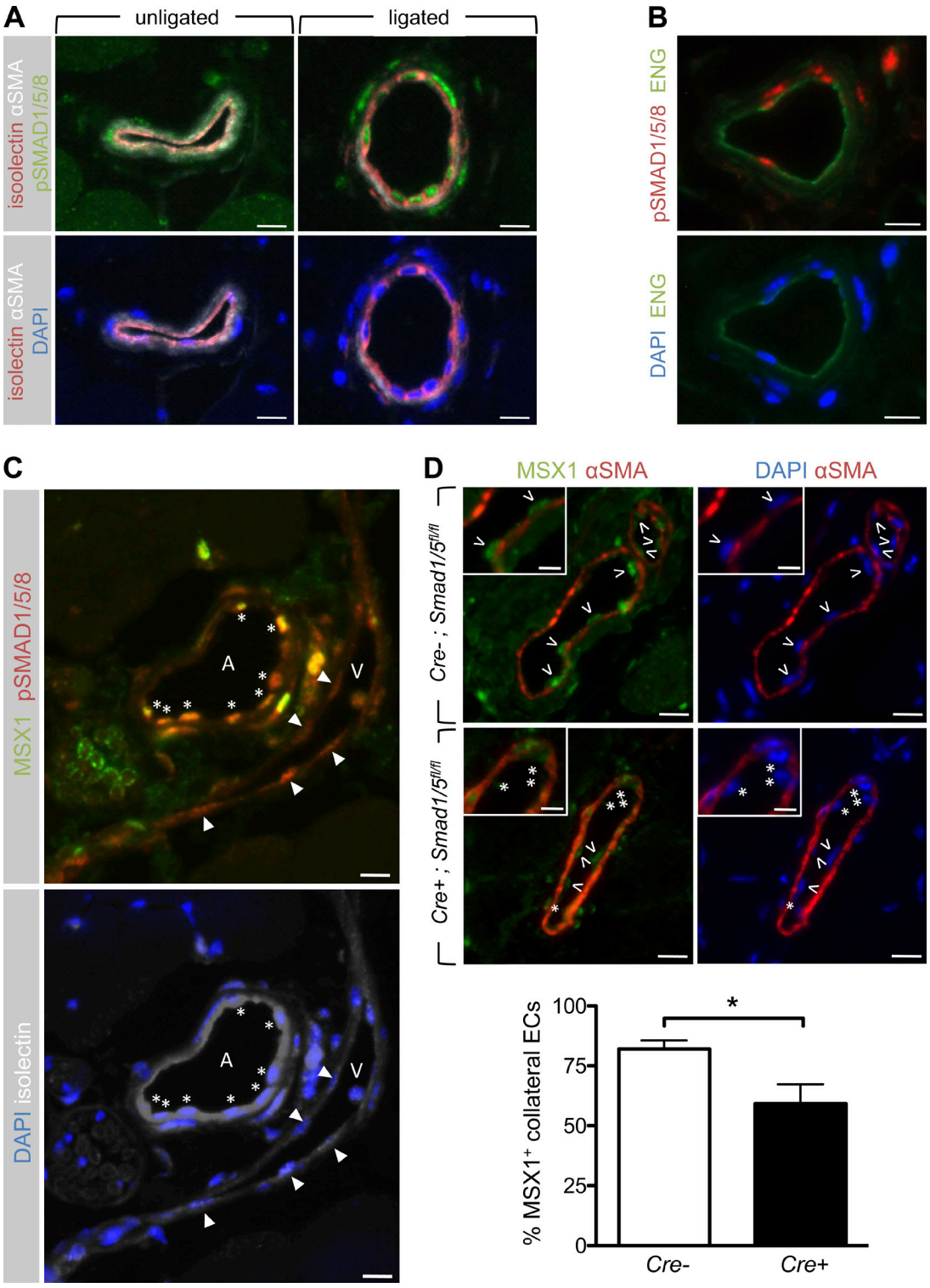

Figure 4. **Canonical BMP signaling is required for endothelial MSX1 induction upon limb ischemia in vivo.** (A) IF staining for pSMAD1/5/8 (green), isolectin GS-IB4 (red), αSMA (white), and DAPI (blue) in unligated (left) and 7-d ligated (right) adductors. (B) Staining for pSMAD1/5/8 (red), ENG (green), and DAPI (blue) in adductor muscle 7 d after ligation. (C) IF staining for MSX1 (green), pSMAD1/5/8 (red), isolectin GS-IB4 (white), and DAPI (blue) in adductor muscles 7 d after ligation. The asterisks indicate double-positive arterial ECs, and arrowheads point at venous ECs only positive for pSMAD1/5/8. A, artery; V, vein. (D) Staining for MSX1 (green), αSMA (red), and DAPI (blue) in the adductor muscle of tamoxifen-treated *Cdh5-CreERT2;Smad1*$^{fl/fl}$*:Smad5*$^{fl/fl}$ mice 7 d after ligation. The arrowheads and asterisks indicate ECs positive and negative for MSX1, respectively. Quantification is represented as percent MSX1-positive collateral ECs. Error bars represent the SEM. $n = 7$ *Cdh5-Cre−;Smad1*$^{fl/fl}$*:Smad5*$^{fl/fl}$ mice and $n = 9$ *Cdh5-*Cre+;*Smad1*$^{fl/fl}$*:Smad5*$^{fl/fl}$ mice. *, $P < 0.05$ versus *Cdh5-Cre−;Smad1*$^{fl/fl}$*:Smad5*$^{fl/fl}$ mice. Bars: (A–C) 10 µm; (D) 25 µm; (magnifications in D) 12 µm.

To establish the necessity of SMAD1/5/8 activity for MSX1 induction in vivo, we subjected mice with EC-specific deletions of *Smad1* and *Smad5* to hind limb ischemia. To overcome the embryonic lethality of constitutive EC-specific *Smad1/5* knockouts (Moya et al., 2012), we crossed mice with a tamoxifen-inducible Cre recombinase under control of the EC-specific *Cdh5* promoter (*Cdh5-CreERT2*) with homozygous mice with *loxP*-flanked *Smad1/5* alleles (*Smad1*$^{fl/fl}$*:Smad5*$^{fl/fl}$). To assess knockout specificity, we intercrossed *Cdh5-CreERT2;Smad1*$^{fl/fl}$*:Smad5*$^{fl/fl}$ with *RCE* Cre mice, generating a reporter line expressing GFP upon Cre-mediated recombination. This allowed validation of the EC-specific Cre recombination in Cre-positive mice (Fig. S4 B). We found a significant reduction in MSX1 induction in mice with reduced *Smad1/5* expression upon analyzing the percentage of MSX1-positive ECs in the collateral endothelium after ligation (Fig. 4 D). MSX1 induction was not completely blunted in the knockout mice as a result of incomplete Cre-mediated annihilation of endothelial SMAD expression, representatively quantified for SMAD1 (Fig. S4 C). Together, these data confirm the canonical BMP signaling pathway to be required for endothelial MSX1 induction during arteriogenesis.

Endothelial MSX1 regulates flow-induced collateral arterial remodeling

Given the shear stress–driven MSX1 induction in growing collaterals, we hypothesized that endothelial MSX1 mediates collateral remodeling. EC-specific depletion of MSX1 and -2 was obtained after tamoxifen treatment of *Cdh5-CreERT2;Msx1*$^{fl/fl}$*:Msx2*$^{fl/fl}$ mice in which the effect of unilateral hind limb ischemia was tested. Despite MSX2 not being induced in ECs during arteriogenesis, both *Msx1* and *Msx2* alleles were inactivated to avoid functional compensation by baseline presence of MSX2 in ECs (Fig. 1 B). Knockout specificity and efficacy upon tamoxifen treatment was validated both in *Cdh5-CreERT2;Rosa:LsL-LacZ*$^{fl/+}$ reporter mice by enzymatic Xgal (5-bromo-4-chloro-3-indolyl-β-D-galacto-pyranoside) staining and in *Cdh5-CreERT2;Msx1*$^{fl/fl}$*:Msx2*$^{fl/fl}$ mice by quantification of MSX1 IF staining in collateral ECs (Fig. S5, A and B). Perfusion recovery was assessed by positron emission tomography (PET) analysis (Peñuelas et al., 2007) on the day of ligation, after 7 d—the moment when collateral remodeling peaks (Herzog et al., 2002), and we concomitantly observed an increased MSX1 expression (Fig. 1 A)—and after 14 d. Flow recovery was quantified as the percentage of remaining blood flow in the limb of the operated versus nonmanipulated side. This revealed a significant lower perfusion recovery and a trend toward lower recovery in the hind limb of EC-specific *Msx*-deficient mice on day 7 (Fig. 5, A and B) and day 14 (Fig. S5 C), respectively. To gain insight into the ongoing vascular remodeling in the absence of *Msx*, a 3D microcomputed tomography (micro-CT) reconstruction of the vascular bed (Duvall et al., 2004) in the hind limb 7 d after unilateral ligation was made (Fig. S5 D). A vessel size distribution diagram was generated for both adductors, and the ratio of the ligated versus nonligated side was calculated as a readout for flow-induced outward collateral remodeling. Although Cre-negative mice showed a strong remodeling response in the collateral range as described previously (Scholz et al., 2002; Li et al., 2006), this response was abrogated in EC-specific *Msx*-deficient mice (Fig. 5, C and D). Together, these results indicate the functional importance of endothelial MSX1 expression in flow-induced outward collateral remodeling.

MSX1 activates the inflammatory response to shear stress in collateral endothelium

The shear stress–induced proinflammatory endothelial state and subsequently recruited monocytes/macrophages are crucial initiators of the collateral remodeling process (Arras et al., 1998; Pipp et al., 2004). Therefore, we questioned whether MSX1 might transduce this extrinsic hemodynamic cue into an inflammatory response in the endothelium. 3 d after arterial occlusion, we observed a significant reduction in CD45-positive leukocyte infiltration around collateral arteries in *Cdh5-CreERT2;Msx1*$^{fl/fl}$*:Msx2*$^{fl/fl}$ adductor muscles (Fig. 6, A and B). By contrast, *Sm22-Cre*–driven *Msx1/2* inactivation did not affect leukocyte infiltration (Fig. 6 C); therefore, MSX1 is required in the EC but not the SMC layer to mediate leukocyte recruitment. To understand the underlying mechanism, we analyzed the expression of the adhesion molecules ICAM1 and VCAM1 in the collateral endothelium of *Cdh5-CreERT2;Msx1*$^{fl/fl}$*:Msx2*$^{fl/fl}$ mice and found both to be reduced in *Msx*-deficient mice 3 d after femoral artery ligation, rendering the endothelium less adhesive for leukocytes (Fig. 6, D–F). Thus, MSX1 is crucial for transducing the extrinsic hemodynamic input into a proinflammatory endothelial state that is required for the recruitment of inflammatory cells; i.e., the instigators of the collateral remodeling process.

Endothelial MSX1 is required for flow-induced ICAM1 and VCAM1 induction through promoter binding

To consolidate the mechanistic link between MSX1 and the proinflammatory endothelial state, we performed gain- and loss-of-function experiments in vitro. Leukocyte adhesion assays revealed an increased monocyte adhesion to MSX1-overexpressing HUAECs, which had a higher *ICAM1* and *VCAM1* expression (Fig. 7, A–C). Interestingly, MSX1 overexpression did not induce *ICAM1* or *VCAM1* expression in SMCs, suggesting that MSX1 does not confer a proadhesive state to these cells (Fig. 7 C), which is in line with our in vivo observations. Furthermore, siRNA-mediated *MSX1* knockdown in HUAECs, which acquired a partially inflamed status upon cell cultivation (Liu et al., 2008), not only reduced expression of *ICAM1* and *VCAM1,* but in addition that of many other arteriogenesis-related proinflammatory genes (Fig. 7 D). Finally, MSX1 expression in ECs was required for the previously reported shear stress–induced *ICAM1* and *VCAM1* expression (Chappell et al., 1998; Sweet et al., 2013) because siRNA-mediated *MSX1* knockdown abrogated their flow-dependent induction (Fig. 7, E and F). Thereby, we confirmed the central role of MSX1 in the transition toward a proinflammatory endothelial phenotype.

To investigate whether MSX1 could affect *ICAM1* and *VCAM1* expression through direct interaction with the *ICAM1* and/or *VCAM1* promoters, we performed chromatin immunoprecipitation (ChIP) assays in HUAECs transduced with Cherry- or FLAG-tagged MSX1-encoding plasmids. To identify putative MSX1 binding regions, we analyzed the epigenome profile of the 20-kb promoter and 5′ untranslated regions in human umbilical cord vein EC (HUVEC) data tracks on the University of California Santa Cruz Genome Browser. Based on the alignment of the activated histone marks H3K27ac, H3K4m1, and/or H3K4m3 and the DNase I sensitive open chromatin mark, we identified four and three potential regulatory elements in the *ICAM1* and *VCAM1* promoters, respectively (Fig. 8, A and B). The repressive mark H3K27me3—previously reported to be enriched on repressed MSX1 target genes in myoblasts (Wang

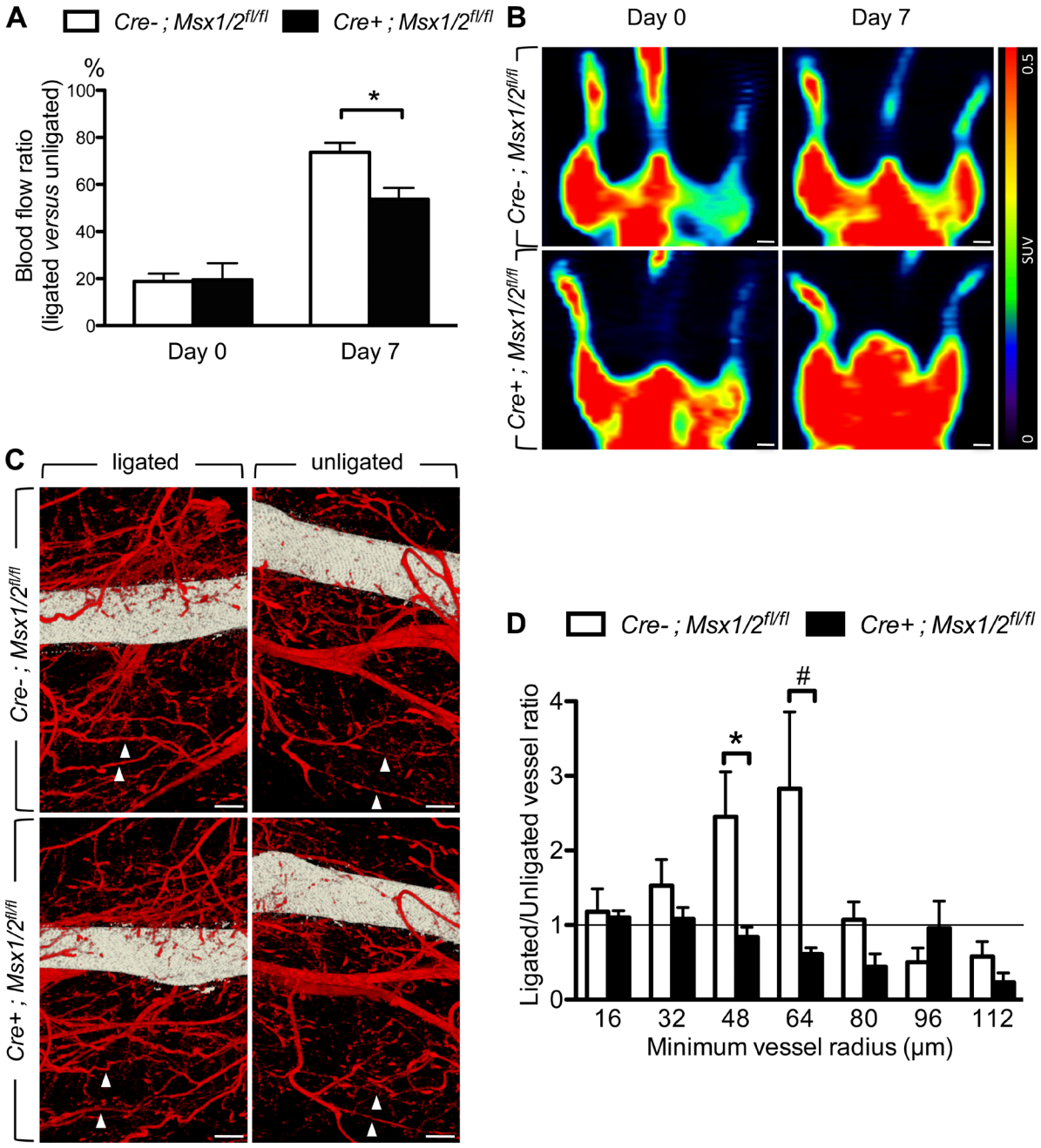

Figure 5. **MSX1 regulates flow-induced outward collateral remodeling.** (A) Upon tamoxifen treatment, *Cdh5-CreERT2;Msx1$^{fl/fl}$:Msx2$^{fl/fl}$* mice were subjected to unilateral femoral artery ligation. Relative flow values were determined by high-resolution PET imaging. Blood flow was quantified as a ratio in the ligated versus the unligated leg, represented as a percentage for $n = 4$ *Cdh5-Cre−;Msx1$^{fl/fl}$:Msx2$^{fl/fl}$* and $n = 3$ *Cdh5-Cre+;Msx1$^{fl/fl}$:Msx2$^{fl/fl}$* littermates. *, $P < 0.05$. (B) Representative PET images of perfusion recovery upon femoral artery ligation in *Cdh5-Cre−* and *Cdh5-Cre+ Msx1$^{fl/fl}$:Msx2$^{fl/fl}$* littermates. (C) Representative micro-CT angiograms of the adductors for both the ligated and unligated hind limbs of *Cdh5-Cre−;Msx1$^{fl/fl}$:Msx2$^{fl/fl}$* (top) and *Cdh5-Cre+;Msx1$^{fl/fl}$:Msx2$^{fl/fl}$* mice (bottom) 7 d after unilateral femoral artery ligation. The arrowheads indicate collateral arteries. (D) Quantification of the amount of blood vessels per size in the micro-CT acquisition of the adductor region 7 d after ligation, represented as the ratio in the ligated versus the unligated adductor. $n = 4$ *Cdh5-Cre−;Msx1$^{fl/fl}$:Msx2$^{fl/fl}$* and $n = 4$ *Cdh5-Cre+;Msx1$^{fl/fl}$:Msx2$^{fl/fl}$* mice. #, $P = 0.076$; *, $P < 0.05$ versus *Cdh5-Cre−;Msx1$^{fl/fl}$:Msx2$^{fl/fl}$* mice. The solid line indicates the 1 ratio, which correlates with no remodeling. Error bars represent the SEM. Bars: (B) 3 mm; (C) 800 µm.

et al., 2011)—was not enriched in these elements. When comparing the anti-FLAG–precipitated DNA regions of interest in FLAG-MSX1-transduced to Cherry-transduced HUAECs, we found FLAG-MSX1 enrichment at the predicted binding site 1 for *ICAM1* and site 2 for *VCAM1*. As a negative control, we simultaneously performed a ChIP assay with mouse IgG antibody and included negative control primers in the quantitative analysis, which did not show enrichment (Fig. 8, C–F). Interestingly, the enriched site of the *ICAM1* promoter was also in the vicinity of a predicted MSX1 binding site identified by the JASPAR TF binding profile database (Sandelin et al., 2004). Thus, MSX1 transduces the endothelium to a proinflammatory state by inducing ICAM1 and VCAM1 expression through a direct interaction with their promoters.

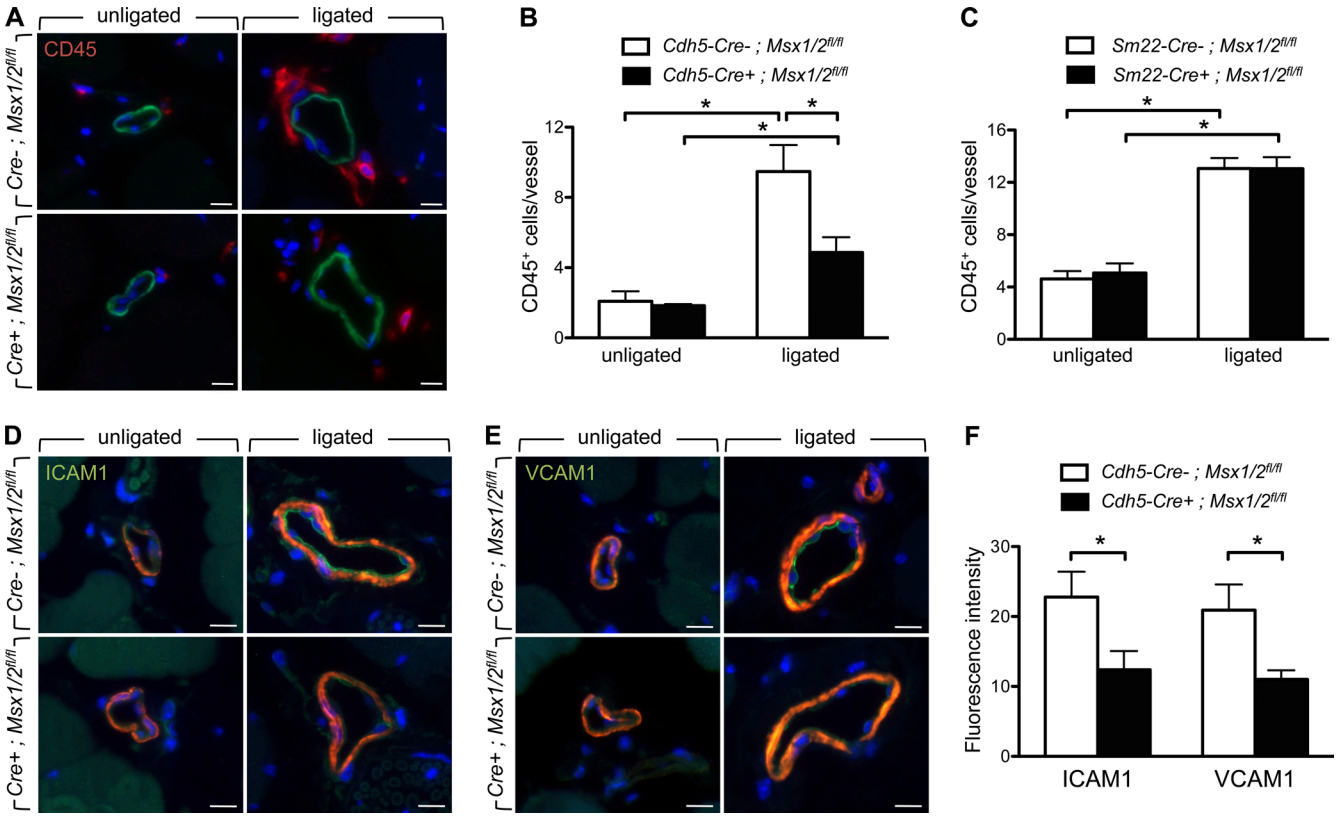

Figure 6. **MSX1 activates the collateral endothelium to a proadhesive state for leukocyte infiltration.** (A) Staining for CD45 to mark leukocytes (red), αSMA (green), and DAPI (blue) in collateral arteries of tamoxifen-treated *Cdh5-CreERT2;Msx1$^{fl/fl}$:Msx2$^{fl/fl}$* mice 3 d after surgery. (B and C) Quantification of leukocyte infiltration in the perivascular region of collateral arteries in *Cdh5-CreERT2;Msx1$^{fl/fl}$:Msx2$^{fl/fl}$* (B) and *Sm22-Cre;Msx1$^{fl/fl}$:Msx2$^{fl/fl}$* mice (C) 3 d after surgery. Data represent the number of CD45-positive cells per vessel. $n = 4$ *Cdh5-CreERT2-;Msx1$^{fl/fl}$:Msx2$^{fl/fl}$*; $n = 5$ *Cdh5-CreERT2+;Msx1$^{fl/fl}$:Msx2$^{fl/fl}$*; $n = 4$ *Sm22-Cre–;Msx1$^{fl/fl}$:Msx2$^{fl/fl}$*; and $n = 4$ *Sm22-Cre+;Msx1$^{fl/fl}$:Msx2$^{fl/fl}$* mice. *, $P < 0.05$ versus the indicated condition. (D and E) Representative stainings for ICAM1 (D) and VCAM1 (E) in green, αSMA (red), and DAPI (blue) in the adductor of tamoxifen-treated *Cdh5-CreERT2;Msx1$^{fl/fl}$:Msx2$^{fl/fl}$* mice 3 d after ligation. (F) Corresponding quantification of the fluorescence intensity for ICAM1 and VCAM1 in the intima of collateral arteries. Data are represented as fluorescence intensity per intimal area (square micrometers). $n = 4$ *Cdh5-CreERT2;Msx1$^{fl/fl}$:Msx2$^{fl/fl}$* and $n = 5$ *Cdh5-CreERT2+;Msx1$^{fl/fl}$:Msx2$^{fl/fl}$* mice. *, $P < 0.05$. Error bars represent the SEM. Bars, 10 µm.

Discussion

During adaptive arteriogenesis, an arterial shear stimulus activates the endothelium, leading to a whole-vessel outward remodeling response. Here, we show that MSX1 is an arterial-specific TF downstream of BMP–SMAD signaling translating this extrinsic cue into a change in the EC status, leading to leukocyte infiltration and collateral remodeling (Fig. 9).

The functional role of the MSX family has been documented during development of a broad range of tissues, including neural tissues, limbs, and craniofacial bone and teeth (Satokata and Maas, 1994; Satokata et al., 2000; Bach et al., 2003; Lallemand et al., 2005); however, its function in the vasculature is less clear. Lopes et al. recently described MSX1 and MSX2 to be involved in the incorporation of neural crest–derived precursors in the medial layer but found no functional role for endothelial MSX1/2 during embryonic vascular development (Lopes et al., 2011) nor in postnatal retinal sprouting angiogenesis (Lopes et al., 2012). Here, we showed MSX1 to exhibit an exclusive arterial expression pattern, which is conserved in developing mice, in line with previous publications (Goupille et al., 2008; Lopes et al., 2011; Aranguren et al., 2013). However, we and others found that endothelial MSX1 expression is not maintained throughout adulthood (Goupille et al., 2008; Lopes et al., 2012), suggesting it has no homeostatic role. Often, expression programs active during vessel development become reactivated during pathological conditions (Cines et al., 1998). Therefore, we assessed the role of MSX1 in hind limb ischemia, a vascular occlusive disease that specifically affects the arterial vascular bed. Within remodeling collateral arteries, we found a strong induction of endothelial MSX1 expression in response to increased shear stress, the main trigger of collateral remodeling (Pipp et al., 2004). The strong dependence of MSX1 expression on its environment was also evident from our previous work showing that freshly isolated arterial ECs lose *MSX1* expression abruptly when deprived of environmental cues in the culture dish (Aranguren et al., 2013). We demonstrate here that hemodynamic changes are the key environmental factors driving endothelial MSX1 expression both in vitro and in our in vivo flow-induced arteriogenic remodeling model.

MSX1 is a target of the canonical BMP signaling pathway. Therefore, we investigated its intracellular receptor-regulated SMAD1/5/8 component during arteriogenesis. We identified pSMAD1/5/8 as an appealing candidate for MSX1 induction during flow-mediated collateral remodeling because transient and persistent SMAD1/5/8 phosphorylation was reported upon exposure of endothelium to LSS or oscillatory conditions, respectively (Zhou et al., 2012). Hence, its activation occurs specifically during changes in the endothelial hemodynamic

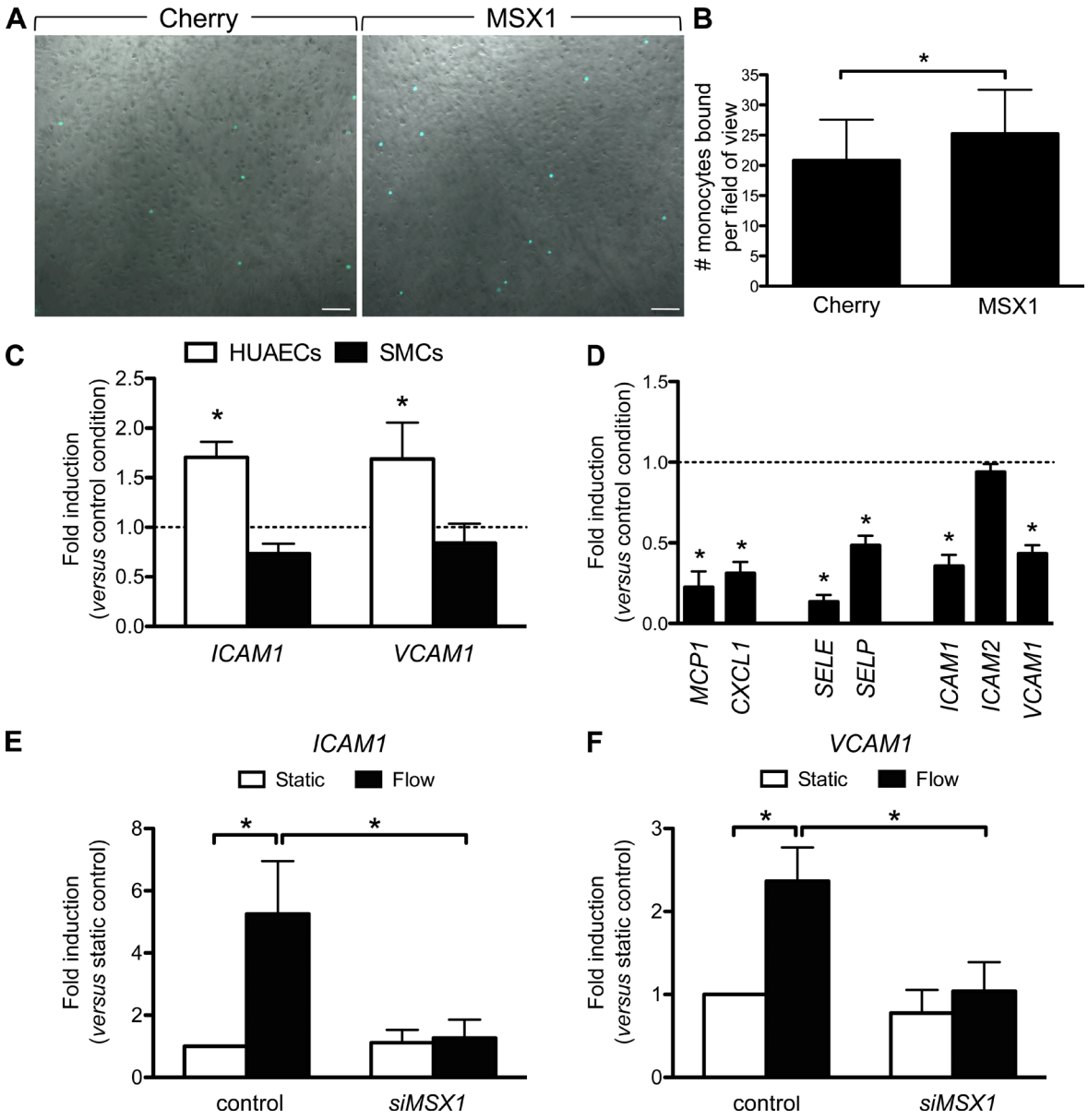

Figure 7. **MSX1 induces an inflammatory proadhesive endothelial state.** (A) Pictures of THP1 cells (in green) attached to HUAECs upon transduction with control Cherry or MSX1 plasmid for 3 d. Bars, 100 µm. (B) Quantification is represented as the number of monocytes per field of view. $n = 6$. *, $P < 0.05$ versus the Cherry control condition. (C) qRT-PCR expression analysis of *ICAM1* and *VCAM1* in MSX1 overexpression conditions mediated by plasmid transduction of HUAECs ($n = 10$) or SMCs ($n = 3$). *, $P < 0.05$ versus the Cherry control condition. (D) qRT-PCR analysis upon siRNA-mediated *MSX1* knockdown. mRNA expression is represented relative to the control condition. $n = 5–7$. *, $P < 0.05$ versus the corresponding control condition. (E and F) qRT-PCR analysis on HUAECs transfected with control siRNA or siRNA against *MSX1* seeded in fibronectin-coated chambers and subsequently kept under static conditions or subjected to 6 h of oscillatory flow. *ICAM1* and *VCAM1* expression is represented relative to the control static condition. $n = 4$ and $n = 3$, respectively. *, $P < 0.05$ versus the indicated condition. Error bars represent the SEM.

environment, in accordance with our observations for MSX1. In the unligated adductor, SMAD1/5/8 exhibited a low activation level, both in arterial and venous ECs as described in other models (Moya et al., 2012; Zhou et al., 2012). Upon femoral artery ligation, pSMAD1/5/8 was specifically induced in the three vascular layers of the collateral arteries, in line with the reported pSMAD1/5/8 activation in the three vascular layers of atherosclerotic lesions (Derwall et al., 2012), another disease model triggered by changing hemodynamic conditions. This endothelial activation of SMAD1/5/8 signaling appeared to be essential for MSX1 induction during arteriogenic remodeling because we showed less MSX1 induction in the remodeling collateral endothelium upon EC-specific knockout of *Smad1/5* in adult mice. Given their ubiquitous expression in arterial and venous ECs, the role of SMAD1/5 signaling in adult mice likely goes beyond arteriogenic remodeling, and a full exploration of this role requires additional studies that exceed the scope of our study on MSX1. At the receptor level, we found that ALK6 and BMPR2 team up to mediate MSX1 induction through SMAD1/5/8 activation, in accordance with a recent publication that linked these receptors in vitro to the shear-driven activation of pSMAD1/5/8 (Zhou et al., 2013). We further provide pioneering mechanistic evidence of ENG as an indispensable receptor in the BMP-mediated endothelial shear response. All together, we identified

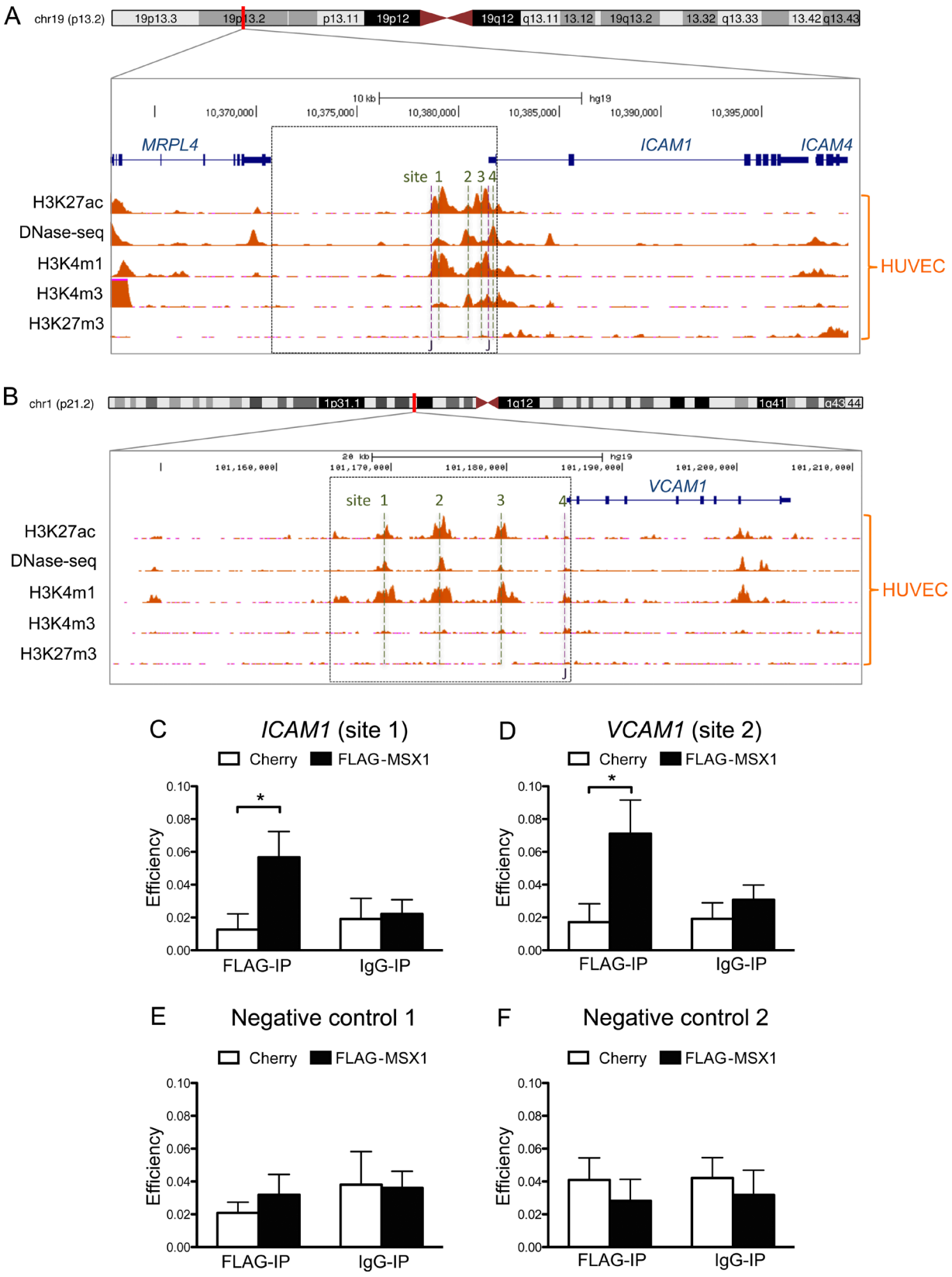

Figure 8. **MSX1 directly binds to the *ICAM1* and *VCAM1* promoter.** (A and B) Epigenome profiling of the *ICAM1* (A) and *VCAM1* (B) promoter representing DNase-seq and ChIP-seq against H3K27ac, H3K4m1, H3K4m3, and H3K27m3 data tracks from the University of California, Santa Cruz Genome Browser of the *ICAM1* and *VCAM1* promoter in HUVECs. Dotted lines show regions of interest, and J indicates predicted MSX1 binding sites from the JAS PAR TF binding profile database. (C–F) qRT-PCR analysis for *ICAM1* (site 1), *VCAM1* (site 2), and two negative control genomic regions upon FLAG- or mouse IgG–based ChIP in HUAECs transduced with Cherry or FLAG-MSX1 plasmid. Data are represented as efficiency of the ChIP assay. Error bars represent the SEM. $n = 6$. *, $P < 0.05$ versus the indicated condition.

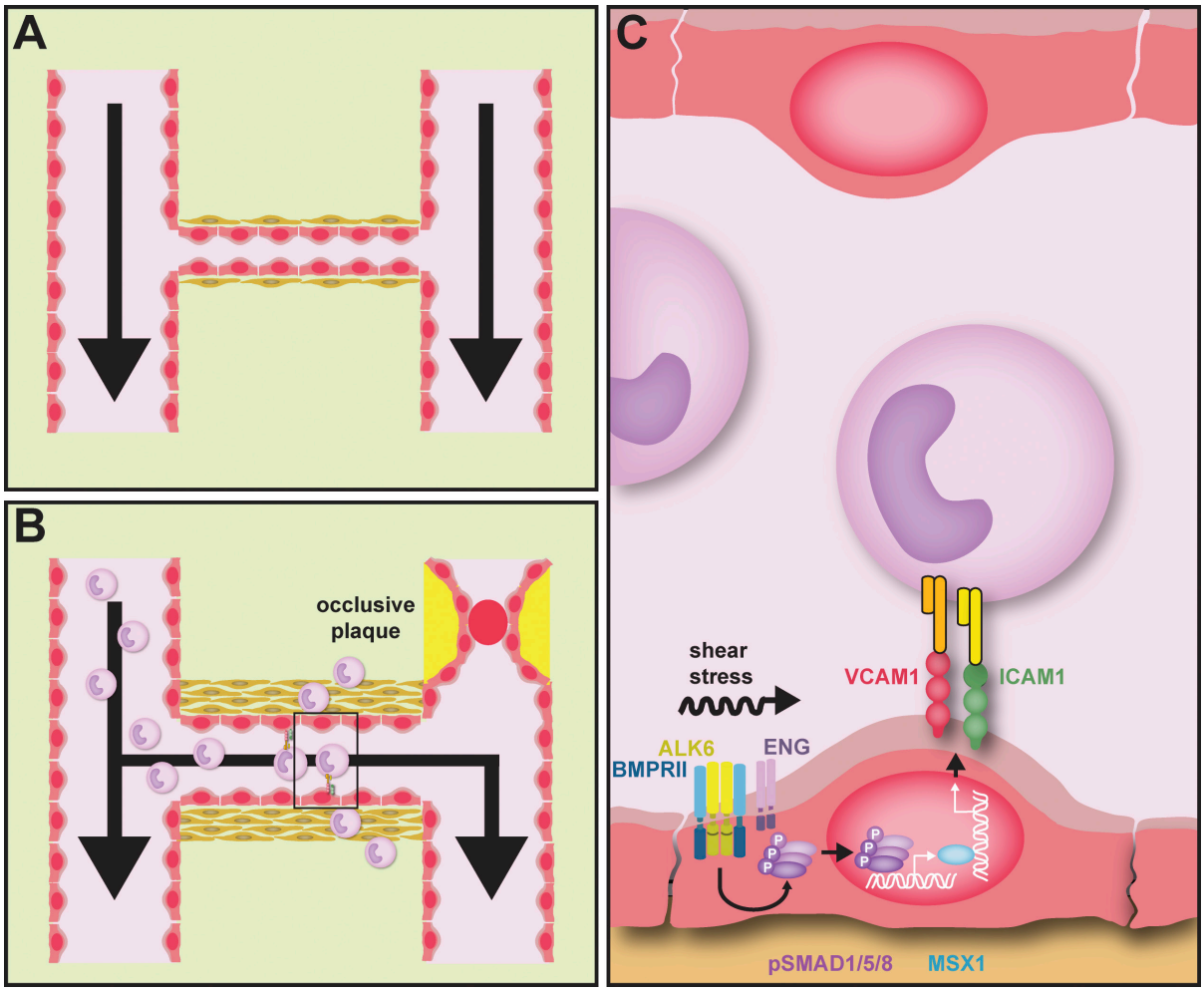

Figure 9. **Graphical summary.** (A–C) During arteriogenic remodeling, an arterial shear stimulus reactivates the endothelium of preexisting collateral arterioles (A), leading to an inflammation-driven whole-vessel outward remodeling response (B and C). Increased shear stress, the primary extrinsic trigger of arteriogenesis, induces the reexpression of MSX1 in the collateral endothelium upon femoral artery ligation, and this reexpression is mediated through an ALK6/BMPR2/ENG–pSMAD1/5/8 signaling cascade. MSX1 subsequently drives endothelial activation toward a proinflammatory state by transcriptionally activating ICAM1 and VCAM1 expression, which render the ECs proadhesive for infiltration of leukocytes, mediating outward collateral remodeling.

that shear-driven MSX1 induction is critically dependent on the ALK6/BMPR2/ENG–pSMAD1/5/8 cascade.

Although SMAD1/5/8 mediates shear-driven MSX1 induction, pSMAD1/5/8 activity did not mirror MSX1 expression, as the latter was only present in collateral arterial ECs, whereas pSMAD1/5/8 was active both in arterial and venous ECs. This is most plausibly the result of a critical threshold of pSMAD1/5/8 signaling necessary for MSX1 induction, which is only reached in collateral arterial ECs as a result of the flow-induced up-regulation of pSMAD1/5/8 activity. This BMP gradient-to-threshold conversion model for MSX1 induction has been shown in telencephalic dorsal midline development (Hu et al., 2008). Alternatively, differential oligomerization resulting from expression, localization, and/or lateral mobility at the receptor level might be responsible for the differential BMP signaling outcome in arterial versus venous ECs (Guzman et al., 2012). Furthermore, this might not only be related to BMP receptors, but also to their interaction with integrins (Zhou et al., 2013) and the mechanosensory complex (Rudini et al., 2008), two other signaling components at the cell membrane responsible for the flow-induced activation of collateral ECs (Cai et al., 2009; Chen et al., 2010). As described in other tissues, a third regulatory level might be an arterial- or venous-specific factor that potentiates or represses downstream signaling by modulating receptor internalization (Kim et al., 2012) or pSMAD1/5/8 complex transcriptional activity (Weng et al., 2012).

To identify an endothelial function for MSX1 during adaptive arteriogenesis, we used two highly sensitive techniques. PET imaging allowed us to gain insight in subtle flow changes in the hind limb, revealing a reduced flow recovery in EC-specific *Msx1/2* knockout mice. To understand the structural differences underlying this reduced flow recovery, we made a micro-CT reconstruction of the vascular bed in the adductor region, quantified vessel size distribution of the ligated versus nonligated side, and found MSX to be indispensable for outward collateral remodeling occurring after femoral artery ligation. Adaptive arteriogenesis is triggered by shear stress and further driven by the activated ECs, which become more adhesive for leukocytes. Expression of ICAM1 and VCAM1, adhesion molecules necessary for leukocyte attachment, has been previously related to BMP activity (Helbing et al., 2011; Pi et al., 2012). Here, we provide the first functional and mechanistic evidence linking shear-induced canonical BMP signaling to a proinflammatory endothelial state by identifying MSX1, a flow-induced down-

stream transcriptional mediator of the BMP-driven proadhesive endothelial phenotype. Upon femoral artery ligation, lowered ICAM1 and VCAM1 expression hampered leukocyte infiltration and hence outward collateral remodeling in EC-specific *Msx1/2* knockout mice. Complementary in vitro experiments revealed that flow-induced induction of ICAM1 and VCAM1 was dependent on MSX1 through its binding to their promoters.

Although our in vivo experiments in EC-specific *Msx1/2* knockout mice revealed a key role in ECs for MSX1 downstream of BMP signaling in inflammatory conversion, MSX1 was also induced in the medial layer of remodeling collateral arteries, likely through BMP signaling. However, MSX1's functional role in SMCs and the way its expression is linked to BMP signaling in these cells was different from ECs. Indeed, unlike in ECs, altering MSX1 expression in SMCs did not affect leukocyte adhesion in vivo, nor their expression of ICAM1 or VCAM1 in vitro. Furthermore, whereas BMP2/6 ligands—the expression of which was triggered by shear in ECs—induced MSX1 expression in SMCs, they did not in ECs. These data are in agreement with the previously reported BMP2/BMP6-triggered MSX1 expression in differentiated SMCs (Hayashi et al., 2006). Furthermore, these observations may explain why Zhou et al. (2012) found that under altered shear stress, Noggin infusion and hence BMP2/4/6 ligand sequestration resulted in abrogation of BMP signaling in SMCs, but not in ECs.

In conclusion, we identified MSX1 as a key arterial-specific endothelial transcriptional mediator during arteriogenesis, transducing the extrinsic shear cue into an inflammation-mediated vascular remodeling response. This study emphasizes the importance of the EC layer to appropriately adapt to pathological conditions because upon a changing environmental cue, EC reactivation can initiate a whole-vessel remodeling response. Furthermore, our findings significantly contribute to understanding the molecular mechanisms underlying the arterial-specific response in PAD, which could form the basis for development of novel therapeutic strategies tailored to specifically trigger an arterial response to boost blood flow recovery in PAD patients.

Materials and methods

EC isolation

HUAECs and HUVECs were isolated from umbilical cords obtained at UZ Leuven Gasthuisberg according to the guidelines of the UZ Leuven Medical Ethics Committee and after informed consent. First, vessels were flushed with PBS to rinse out the blood and subsequently filled with 0.2% collagenase type I (Gibco) dissolved in 0.9% NaCl with 2 mmol/liter $CaCl_2$ and incubated at 37°C for 12 min to detach the ECs. EC-containing collagenase suspension was collected by flushing the vessels with PBS with 1% FBS, filtered through a 40-µm cell strainer, spun down at 600 *g* for 7 min, and plated on flasks precoated with 0.1% gelatin (Sigma-Aldrich) in EGM-2MV medium supplemented with the CC-4147 Bulletkit (Lonza) and 1% penicillin/streptomycin (Life Technologies). Collection for microarray analysis was performed in collaboration with the University of Navarra, Pamplona and analyzed as reported previously (Aranguren et al., 2013).

In vitro experiments

Flow. Freshly isolated HUAECs or HIAECs (ATCC) were seeded at a density of 24,000 cells/cm^2 on fibronectin-coated flow chambers (µ-Slide $VI^{0.4}$; ibidi) and after cell attachment were connected through a tubing system consisting of BPT tubing (2-Stop PharMed; Cole-Parmer) and silicone tubing (Tygon; Metrohm) to a microprocessor-controlled dispensing pump (IPC ISM934; Ismatec) or a syringe pump system (Harvard Apparatus) for laminar and oscillatory flow, respectively (provided by J. Schrooten, Prometheus, KU Leuven, Belgium). We added a bubble trap to the laminar flow circuit in order to avoid any flow disturbances resulting from bubbles in the flow chamber and applied different shear stresses over time. The syringe pump was programmed to 0 ± 5 dynes/cm^2 at 1 hz for 6 h using EZ PRO software (Harvard Apparatus). The required flow rate (Ø) for the different shear stresses (τ) was calculated according to the following equation in which we used the viscosity (η) for water at 37°C as an approximation for the viscosity of the circulated medium at 37°C as previously described (van der Meer et al., 2010). The constant value in the equation takes the dimensions of the used flow chamber into account, according to the manufacturer's instructions (ibidi).

$$\tau\left(\frac{\text{dynes}}{\text{cm}^2}\right) = \eta\left(\frac{\text{dynes} \times \text{s}}{\text{cm}^2}\right) \times 176.1 \times \phi\left(\frac{\text{ml}}{\text{min}}\right)$$

siRNA knockdown. HUAECs were seeded in 6-well plates, at a density of 25,000 cells per well for MSX1 and 100,000 cells per well for SMAD1/5 and ENG conditions and corresponding control conditions. Subsequently, cells were transfected with 8.3 nmol/liter *siMSX1* (s8999; Invitrogen), 5 nmol/liter *siSMAD1* and *siSMAD5* (L-011026-00-0005 and L-012723-00-0005; Thermo Fisher Scientific), 5 nmol/liter *siENG* (L-015791-00-0005; Thermo Fisher Scientific), or the corresponding concentration of control siRNA (am4636; Invitrogen) dissolved in Opti-MEM (Invitrogen) supplemented with Lipofectamine 2000 (Invitrogen). For *ALK6* (s2041; Invitrogen) and *BMPR2* (s2044; Invitrogen) knockdown experiments, 100,000 cells were seeded and transfected with 10 nmol/liter siRNA or the corresponding concentration control siRNA in Opti-MEM supplemented with Lipofectamine RNAiMAX (Invitrogen). After overnight incubation with the siRNAs, cells were washed and reseeded in fibronectin-precoated flow chambers, and upon cell attachment were exposed to 1 h of shear stress or kept in static conditions as the control. Only for *MSX1* knockdown experiments were cells washed the next day and reseeded one additional day later. To inhibit ALK1/2/3 signaling, 2.5 µmol/liter DMH1 inhibitor (Sigma-Aldrich) or the corresponding DMSO volume as a control was added to the medium 1 h before onset of flow and during flow exposure and according to the static condition. After exposure to flow, cells were lysed with TRIzol reagent (Invitrogen) or with radioimmunoprecipitation assay buffer (Sigma-Aldrich) for analysis at the mRNA or protein level, respectively.

Transduction. HUAECs were seeded in 24-well plates at a density of 80,000 cells per well. Subsequently, cells were transduced with 0.5 µg Cherry, MSX1, or FLAG-MSX1 plasmid dissolved in Opti-MEM supplemented with FuGENE HD transfection reagent (Promega). After 3 d, cells were used for expression analysis (after lysis in TRIzol reagent), monocyte attachment, or ChIP assay.

Hypoxia. HUAECs were seeded in gelatin-coated wells and kept in 21% (normoxia) or 1% oxygen (hypoxia) for 3 d, after which cells were lysed with TRIzol reagent for expression analysis.

BMP ligands. Freshly isolated HUAECs and uterine SMCs (Lonza) were seeded in 6-well plates at a density of 40,000 and 20,000 cells per well, respectively. Subsequently, cells were serum starved for 1 h, and rBMP2 (355-BM; R&D Systems), rBMP6 (a gift from S. Vukicevic, Genera Research, Zagreb, Croatia), or the corresponding solute was added at a concentration of 10 ng/ml for 48 h, after which cells were lysed with TRIzol reagent for expression analysis.

Monocyte attachment assay. THP1 cells (ATCC) were grown in suspension in RPMI 1640 medium (Life Technologies) supplemented with 1-mM sodium pyruvate (Life Technologies), 10% FBS, and 1%

penicillin/streptomycin (Life Technologies). THP1 cells were spun down and resuspended in serum-free RPMI 1640 medium with 1-µM CellTracker green (Life Technologies) and incubated for 20 min at 37°C. HUAECs were washed with RPMI medium and subsequently exposed to washed THP1 cells in a 1:1 ratio. After a 25-min incubation at 37°C, the unbound THP1 cells were removed by washing steps, after which the attached THP1 cells on the EC monolayer were fixed with 4% PFA for 10 min. Five pictures per well were taken at a 5× magnification, and the number of attached THP1 cells per field of view was analyzed.

ChIP. HUAECs were transduced with Cherry or FLAG-MSX1 plasmid, and after 3 d ChIP was performed using the Transcription ChIP kit (Diagenode) according to the manufacturer's instructions. Chromatin was sheared during eight consecutive cycles of 30-s high-intensity shearing with a sonication device (Bioruptor; Diagenode). Subsequently, one third of the sample was stored as an input sample. The remaining sheared chromatin was divided in two and incubated with 2.5 µg monoclonal anti-FLAG M2 antibody (F1804; Sigma-Aldrich) or mouse IgG (C15400001; Diagenode) overnight. Finally, the immunoprecipitated DNA samples were analyzed by qRT-PCR using primers designed against ICAM1, VCAM1, a negative control provided by the manufacturer (Diagenode), and an additional negative control for a gene desert in chromosome 12 (negative control 2; Table 1). ChIP efficiency of a particular genomic locus was determined as a percentage of the starting material (input) by calculating $2\text{^}(C_T \text{ input} - C_T \text{ ChIP})$ multiplied by the applied dilution factor of the input sample according to the manufacturer's instructions.

In vivo experiments

Mice. C57BL/6 mice (The Jackson Laboratory) were used as the wild-type strain (e.g., for expression studies). The inducible endothelial-specific *Cdh5-CreERT2* driver line was created by recombining the tamoxifen-inducible *CreERT2* fragment into the start codon of the genomic *Cdh5* sequence using a P1 artificial chromosome, as described previously (Wang et al., 2010). The transgenic construct for the generation of the constitutive *Sm22-Cre* driver line was obtained by ligating the smooth muscle–specific *Sm22* promoter to a bacteriophage P1 Cre recombinase–containing plasmid (Holtwick et al., 2002). To assess the endothelial function of MSX1, we intercrossed *Cdh5-CreERT2* mice (provided by R. Adams, Max Planck Institute for Molecular Biomedicine, Münster, Germany) and *Sm22-Cre* mice (provided by A. Zwijsen, KU Leuven, Belgium) with mice with loxP sites flanking the homeodomain-encoding second exons of *Msx1* and *Msx2* (*Msx1*$^{fl/fl}$*:Msx2*$^{fl/fl}$ mice; provided by R. Maxson, Keck School of Medicine of the University of Southern California, Los Angeles, CA; Fu et al., 2007). To analyze the pathway mediating shear-induced MSX1 induction, the *Cdh5-CreERT2* mice were also intercrossed with mice with loxP sites flanking the first and second coding exon of the *Smad1* and *Smad5* genes, respectively (*Smad1*$^{fl/fl}$*:Smad5*$^{fl/fl}$ mice; provided by A. Zwijsen; Tremblay et al., 2001; Umans et al., 2003). Cre activity was induced in the adult endothelium by intraperitoneal injection of 2 mg tamoxifen (Sigma-Aldrich) for five consecutive days, and after 2 d of rest the femoral artery was ligated. Tamoxifen was dissolved in a sunflower seed oil/ethanol (10:1) mixture at 30 mg/ml, sonicated, and diluted in sunflower seed oil to a working solution of 10 mg/ml, which was preheated before injection. Knockout efficiency was analyzed in *Cdh5-CreERT2* mice intercrossed with *Rosa:LsL-LacZ*$^{fl/+}$ (The Jackson Laboratory) or *RCE* Cre reporter lines (provided by A. Zwijsen). The *Rosa:LsL-LacZ*$^{fl/+}$ reporter strain was generated by cloning a loxP-flanked DNA STOP sequence upstream of the *LacZ* gene in the *Rosa26* locus. The *RCE* Cre strain was generated by the homologous recombination of a dual stop-EGFP cassette, containing a loxP-flanked *pGK-Neo-pA* cassette, upstream of the hybrid CAG promoter-driven EGFP reporter in the *Rosa26* locus (Sousa et al., 2009). All animal procedures were approved by the Animal Ethics Committee of KU Leuven.

Surgery. Femoral artery ligation was performed in 8–12-wk-old mice, which were anesthetized with an intraperitoneal injection of 1.2% ketamine and 1% xylazine in saline and placed on a heating pad at 37°C. The skin was disinfected with 70% ethanol and iodine disinfectant solution before incision. Subsequently, the femoral artery of the right limb was ligated as previously described (Buschmann et al., 2010). The incision was stitched and disinfected with iodine. Mice were kept on the heating pad until they were awake and were treated postoperatively with the analgesic buprenorphine, which was administered at 0.1 mg/kg subcutaneously for up to 1 wk after the procedure.

Sample processing for histology. On the day of sacrifice, mice were sedated with the ketamine/xylazine/NaCl mixture, upon which vessels were perfused first with 0.2% adenosine (Sigma-Aldrich) to induce vasodilation and then with Zinc Fix for fixation. Adductor and gastrocnemius muscles were dissected and fixed in Zinc Fix overnight, upon which they were washed with distilled water and transferred to 70% ethanol. Samples were run overnight through a tissue processor (TP1020; Leica), embedded in paraffin, and sectioned at 5 µm with a microtome (HM360; Microm).

Micro-CT. For micro-CT analysis, mice were sedated 7 d after ligation with the ketamine/xylazine/NaCl mixture and subsequently perfused first with 0.2% adenosine for vasodilation, then with 4% PFA for fixation, and then with saline to wash out the fixative, followed by a preheated solution of 30% barium sulfate (Micropaque; Guerbet) in 2% gelatin. To solidify the gelatin and fix the contrast agent in the vessels, mice were stored on ice at 4°C overnight. The next day, limbs were dissected out and stored in PBS. Subsequently, the hind limbs were imaged with a micro-CT system (SkyScan 1172; Bruker microCT) with a peak tube voltage of 50 kV, a current of 200 mA, a filter of 0.5 mm aluminum, and an exposure time of 590 ms. The dataset was reconstructed using the Feldkamp–Davis–Kress algorithm of the manufacturer (NRecon; Bruker microCT) into a 3D image with an isotropic voxel size of 8 µm. The image was analyzed and quantified using custom-made software developed in MeVisLab (MeVis Medical Solutions AG and Fraunhofer MEVIS, Bremen, Germany) and was downsampled by a factor of two for reasons of computational feasibility. A volume of interest (VOI) containing the vascular network of the adductor region was delineated by consistently using landmarks of the femur as proximal and distal boundaries. The bone was manually delineated and removed from the VOI. The blood vessels in the VOI were segmented using hysteresis thresholding, and fragments smaller than 10 voxels

Table 1. **List of human primers for ChIP**

Gene	Forward primer (5′- to -3′)	Reverse primer (5′- to -3′)
ICAM1	GAGAAAGCTCAGGCCACAAG	AAGAATGGCCTCAGACCAGA
VCAM1	GGGGTTGAGCTGAGTTGAGA	CCTACTCGAAGCCACACAGC
Negative control 2	ATGGTTGCCACTGGGGATCT	TGCCAAAGCCTAGGGGAAGA

were excluded to minimize the influence of noise. The vascular network was skeletonized, and the local vessel radius was determined at each point of the skeleton. The combined skeleton length of blood vessels of a certain thickness was computed and normalized for the femur length, and the ratio of the ligated versus nonligated side was made as readout for flow-induced outward collateral remodeling. For 3D visualization, a downsampling by a factor of six was applied for reasons of computational feasibility.

PET. Mice were anesthetized with 2% isoflurane in oxygen with a flow rate of 1.9 liters/min and injected intravenously with [^{13}N]ammonia (25.05 ± 3.58 megabecquerel). Subsequently, mice were positioned in the lutetium oxyorthosilicate–based microPET system (Focus 220; Concorde Microsystems/Siemens) with a ring diameter of 258 mm, a field of view of 76 mm, and a resolution (full width at half maximum) of 1.3 mm at the center of the field of view. Two mice were placed side by side and scanned simultaneously for 20 min starting 10 min after injection as previously described (Peñuelas et al., 2007). A transmission scan for attenuation correction was performed using a rotating ^{57}Co point source. Projection data were normalized for detector efficiency and corrected for dead time, decay, and attenuation. 3D maximum a posteriori reconstructions were performed in a 128 × 128 × 95–nCi/cc (activity concentration) matrix with an in-plane axial pixel size of 1.9 mm and a trans-axial slice thickness of 0.796 mm. Reconstructed data were corrected for weight and injected dose, allowing a standardized uptake value-based analysis using PMOD 3.1 software. In two planes of the coronal slices of the PET data, the paw was manually delineated, and the mean standardized uptake value was calculated as the measurement of perfusion. Flow recovery was evaluated as the ratio between the right (ligated) and left (unligated) hind limb in both animal groups.

IF staining

Tissues. Paraffin sections of human umbilical cord and mouse adductors were immunofluorescently stained. After deparaffination and rehydration, antigen retrieval was performed by 20 min of boiling in citrate buffer, pH 6, for all antibodies, except for CD45 and MSX2, where target retrieval solution (s1699; Dako) was applied three times for a 5-min microwave heating or a 20-min 100°C oven heating, respectively. After cooling down in TBS, endogenous peroxidase activity was quenched by means of 0.3% H_2O_2 in methanol for staining with amplification. For nuclear factors, an extra permeabilization step of 0.5% Triton X-100 in PBS was added followed by 45 min of blocking in 20% serum/80% TNB solution (0.1-M Tris-HCl, pH 7.5, 0.15 M NaCl, and 0.5% blocking reagent [tyramide signal amplification kit]; PerkinElmer). Primary antibodies against the following proteins or lectins were applied overnight: 1:1,000 mouse anti–smooth muscle α-actin (αSMA; A5228; Sigma-Aldrich), 1:200 mouse anti–αSMA-Cy3 (C6198; Sigma-Aldrich), 1:100 rat anti-CD45 (BD553076; BD), 1:100 goat anti-ENG (AF1320; R&D Systems), 1:100 chicken anti-GFP (ab13970; Abcam), isolectin GS-IB4 conjugated with 1:100 Alexa Fluor 568 or 1:200 Alexa Fluor 647 (121412 and 132450; Life Technologies), 1:100 goat anti-ICAM1 (AF796; R&D Systems), 1:100 goat anti-MSX1 (AF5045; R&D Systems), 1:200 rabbit anti-MSX2 (HPA005652; Sigma-Aldrich), 1:100 rabbit anti-SMAD1 (S9743; Cell Signaling Technology), 1:100 rabbit anti-pSMAD1/5/8 (S9511; Cell Signaling Technology), and 1:100 goat anti-VCAM1 (AF643; R&D Systems). Donkey anti–goat, –rabbit, –mouse, or –rat secondary antibodies were Alexa Fluor 488, 568, or 660 conjugated (1:200; Life Technologies). 1:100 donkey anti–chicken secondary antibodies were conjugated with Alexa Fluor 488 (703-546-155; Jackson ImmunoResearch Laboratories, Inc.) or were biotin conjugated (Santa Cruz; 1:300). Where appropriate, signals were amplified with fluorescein or cyanine-3 tyramide-based amplification systems (PerkinElmer). Slides were sealed with ProLong gold antifade reagent (Life Technologies) with DAPI.

Cells. Cells were washed and fixed for 10 min with 4% PFA. Subsequently, cells were washed with TBS/glycine (composed of 10× stock solution: 38 grams NaCl, 9.38 grams Na_2HPO_4, 2.07 grams NaH_2PO_4, and 37.5 grams glycine), permeabilized with 0.5% Triton in TBS, washed again with TBS/glycine, and incubated with blocking solution (2% BSA in TBS) for 1 h. Subsequently, cells were incubated overnight at 4°C with MSX1 (1:20) and pSMAD1/5/8 (1:100) in blocking solution, washed, incubated with Alexa-conjugated secondary antibody (1:500) for 1 h and, after washing, incubated for 5 min with Hoechst 33253 solution (1:500; Sigma-Aldrich), and washed again. Rinsing steps after incubation with primary antibodies were performed with IF wash buffer (composed of 10× stock solution: 38 grams NaCl, 9.38 grams Na_2HPO_4, 2.07 grams NaH_2PO_4, 2.5 grams NaN_3, 5.0 grams BSA, 10 ml Triton X-100, and 2.5 ml Tween 20).

Enzymatic Xgal staining. Mice were consecutively perfused with 0.2% adenosine and PBS containing 0.2% glutaraldehyde and 2 mmol/liter $MgCl_2$. Adductors were dissected, washed in PBS, and fixed for 20 min with PBS containing 1% formaldehyde, 0.2% glutaraldehyde, and 0.02% NP-40. After three washing steps of 10 min, muscles were whole-mount stained at 30°C with 1 mg/ml Xgal (Life Technologies), 5 mmol/liter $K_3Fe(CN)_6$, 5 mmol/liter $K_4Fe(CN)_6$, and 2 mmol/liter $MgCl_2$ in PBS. After three washes with PBS, muscles were fixed for 2 h in 4% PFA, washed again, and processed for paraffin embedding and sectioning.

Analysis. Images were recorded at room temperature on a microscope (AxioImager Z1; Carl Zeiss) with EC Plan-Neofluar objective lenses at 20× (NA 0.5) and 40× (NA 0.75) magnification and on a fluorescence microscope (Axiovert 200M; Carl Zeiss) with LD Plan-Neofluar objective lenses at 20× (NA 0.4) and 40× (NA 0.6) magnification, both equipped with a camera (AxioCam MRc 5; Carl Zeiss). The acquisition was performed with AxioVision version 4.8 software (Carl Zeiss), and subsequently images were cropped, pseudocolored, and contrast adjusted using Photoshop (Adobe). The collateral arteries within the transversally sectioned adductor region were identified as previously described (Scholz et al., 2002). To quantify the percentage of MSX1-positive collateral ECs in *Cdh5-CreERT2;Smad1$^{fl/fl}$:Smad5$^{fl/fl}$* mice 7 d after ligation, we determined the total number of collateral ECs in transversal sections of the adductor region for each mouse by counting the nuclei (DAPI positive) at the inner side of the αSMA layer and quantified the percentage of these cells that were positive for MSX1. Similarly, in these mice, the number of ECs positive for SMAD1 was counted in transversal sections of the adductor region and expressed relative to the total number of analyzed ECs. To quantify the number of leukocytes in the adventitia of collaterals of *Cdh5-CreERT2;Msx1$^{fl/fl}$:Msx2$^{fl/fl}$* mice 3 d after femoral artery ligation, for each collateral vessel, the number of CD45$^+$ adventitial cells was counted. The IF intensity of ICAM1 and VCAM1 in the intima was quantified in the quantitation software on images taken with a confocal microscope (LSM 700; Leica) with an EC Plan-Neofluar objective lens at 20× (0.5 NA) magnification (Carl Zeiss) applying the same settings to acquire fluorescence intensity within the linear range for all samples.

RNA isolation and qRT-PCR. Cells were lysed and total RNA was extracted and isolated using a TRIzol reagent-based protocol. RNA was isolated and subsequently reverse transcribed using SuperScript III reverse transcriptase (Invitrogen). For expression analysis by qRT-PCR, cDNA was amplified using the primer sequences listed in Table 2 during 40 cycles on a real-time PCR system (StepOnePlus; Applied Biosystems) and detected by intercalation of the fluorescent SYBR green I dye (Applied Biosystems) in the double-stranded DNA. Each measurement was performed in triplicate, and mRNA levels were nor-

malized against *GAPDH* as a housekeeping gene, except for the analysis of hypoxia experiments, where *ACTB* was used as a reference gene.

Western blot

Cells were lysed in radioimmunoprecipitation assay buffer (Sigma-Aldrich) and supplemented with 1:100 protease and phosphatase inhibitor cocktail (Thermo Fisher Scientific). The protein concentration was quantified with the bicinchoninic acid protein assay kit (Thermo Fisher Scientific). Subsequently, samples were mixed with reducing agent (Life Technologies) and lithium dodecyl sulfate sample buffer (Life Technologies), loaded on the gel, and run for 50 min at 200 V. Subsequently, proteins were blotted on a nitrocellulose membrane for 90 min at 80 V, and after staining of the membrane, pictures were taken on a molecular imager (ChemiDoc XRS+; Bio-Rad Laboratories) with Image Lab software (Bio-Rad Laboratories). The following antibodies were used: 1:1,000 GAPDH (14C10; Cell Signaling Technology) as a loading control, 1:200 MSX1 (AF5045; R&D Systems), 1:1,000 SMAD1 (S9743; Cell Signaling Technology), and 1:1,000 pSMAD1/5/8 (S9511; Cell Signaling Technology). Bands were quantified with Image Lab version 4.0 software and normalized relative to the loading control.

Statistics

Data are represented as mean ± SEM. Data comparing two groups were analyzed by means of a two-sided Student's *t* test with equal variance. In vitro time course flow experiments were analyzed with a repeated measures one-way analysis of variance test followed by a Dunnett posthoc test. A two-way analysis of variance with a Bonferroni posttest analysis was applied for the qRT-PCR and Western blot quantification of knockdown experiments in flow conditions. When we statistically analyzed the fold inductions of qRT-PCR and Western blot quantifications by a one-sample Student's *t* test, we indicated the null hypothesis with a dashed line. The monocyte attachment assay was quantified by a paired Student's *t* test. Prism software (GraphPad Software) was used for all statistical analysis, and a p-value <0.05 was considered significant.

Online supplemental material

Fig. S1 shows that MSX1 exhibits an arterial-specific expression profile in human umbilical cords. Fig. S2 displays triggering cues for *MSX1* expression in ECs. Fig. S3 presents an assessment of shear induction and siRNA-mediated knockdown efficiency. Fig. S4 shows asymmetric pSMAD1/5/8 activity induction and validation of Cre recombination in *Cdh5-CreERT2;RCE:loxP;Smad1$^{fl/fl}$:Smad5$^{fl/fl}$* and *Cdh5-CreERT2;Smad1$^{fl/fl}$:Smad5$^{fl/fl}$* mice. Fig S5 depicts validation of Cre recombination in *Cdh5-CreERT2;Rosa:LsL-LacZ$^{fl/+}$* mice and assessment of Cre recombination, flow, and collateral remodeling in *Cdh5-CreERT2;Msx1$^{fl/fl}$:Msx2$^{fl/fl}$* mice. Online supplemental material is available at http://www.jcb.org/cgi/content/full/jcb.201502003/DC1.

Acknowledgments

We thank R. Maxson for providing *Msx1$^{fl/fl}$:Msx2$^{fl/fl}$* mice, R. Adams for providing *Cdh5-CreERT2* mice, E. Caluwé, B. Hoekman, T. Koninckx, P. Vandervoort, A. Van Santvoort, and T. Vervoort (KU Leuven, Leuven, Belgium) for technical assistance, and D. Huylebroeck (Erasmus MC, Rotterdam, Netherlands) and S. Aerts (KU Leuven) for discussion of the manuscript.

This work was supported by a European Commission grant (FP7-StG-IMAGINED203291) to A. Luttun, a PhD Fellowship of the Research Foundation – Flanders (FWO) to I. Vandersmissen, a Fellowship Fundamental Clinical Investigatorship of the FWO (1803311N) to R. Devlieger, a KU Leuven Geconcerteerde Onderzoeksacties grant (GOA11/012) to A. Luttun and A. Zwijsen, a KU Leuven Program Financing grant (PF/10/014) to A. Luttun, an Interuniversity Attraction Poles grant (IUAP/P7/07) to A. Luttun and A. Zwijsen, and FWO research grants (G.0393.12 and G.0B09.13 to A. Luttun and

Table 2. **List of human primers for qRT-PCR**

Gene	Forward primer (5′- to -3′)	Reverse primer (5′- to -3′)
ACTB	TGGCACCACACCTTCTACAATG	TAGCAACGTACATGGCTGGG
ALK6	CACCCTACACTGCCTCCATT	AAACTTCCCCATAGCGACCT
BMP2	CCCACTTGGAGGAGAAACAA	AGCCACAATCCAGTCATTCC
BMP4	TGAGCCTTTCCAGCAAGTTT	CTTCCCCGTCTCAGGTATCA
BMP6	AACGCACACATGAATGCAAC	GAACCGAGATGGCATTTAGC
BMP7	CTACATGAACGCCACCAACC	AGGATGACGTTGGAGCTGTC
BMP9	ACGTGAAGGTGGATTTCCTG	CTTCTGGAAGGGGAAGTCCT
BMP10	AGCAAGACGGTGTCGACTTT	TTCATGGTGAGGAATGGACA
BMPR2	CCATGAGGCTGACTGGAAAT	CATCCTGGTCCCAACAGTCT
CXCL1	ATTCACCCCAAGAACATCCA	TCCTAAGCGATGCTCAAACA
ENG	TGCCACTGGACACAGGATAA	CCTTCGAGACCTGGCTAGTG
GAPDH	TGGTATCGTGGAAGGACTCATGAC	ATGCCAGTGAGCTTCCCGTTCAGC
ICAM1	CGCTGAGCTCCTCTGCTACT	TAGGCAACGGGGTCTCTATG
ICAM2	CTGCACTCAATGGTGAAGGA	AGGTACACGTGAGGCCAAAG
KLF2	CACCAAGAGTTCGCATCTGA	GGCTACATGTGCCGTTTCA
MCP1	GCCTCCAGCATGAAAGTCTC	CAGATCTCCTTGGCCACAAT
MSX1	AGTTCTCCAGCTCGCTCAGC	GGAACCATATCTTCACCTGCGT
SELE	CCTTCCTGCCAAGTGGTAAA	GCTACCAAGGGAATGTTGGA
SELP	ACACCTTTGCTAAGCCCTCA	CTCTGGGGCAAAGAGTTCTG
SMAD1	GGGACTGCCTCATGTCATTT	TTGGGTTGCTGGAAAGAATC
SMAD5	AACCTGAGCCACAATGAACC	GTGGCATATAGGCAGGAGGA
VCAM1	ACACACAGGTGGGACACAAA	GGTGCTGCAAGTCAATGAGA
VEGF	ACCAAGGCCAGCACATAGGA	AGGCCCACAGGGATTTTCTT

G.0542.13 to A. Zwijsen, A. Luttun, and L. Umans). The sponsors of this study are public or nonprofit organizations that support science in general. They had no role in gathering, analyzing, or interpreting the data.

The authors declare no competing financial interests.

Submitted: 2 February 2015
Accepted: 18 August 2015

References

Aird, W.C. 2007. Phenotypic heterogeneity of the endothelium: II. Representative vascular beds. *Circ. Res.* 100:174–190. http://dx.doi.org/10.1161/01.RES.0000255690.03436.ae

Amatschek, S., E. Kriehuber, W. Bauer, B. Reininger, P. Meraner, A. Wolpl, N. Schweifer, C. Haslinger, G. Stingl, and D. Maurer. 2007. Blood and lymphatic endothelial cell-specific differentiation programs are stringently controlled by the tissue environment. *Blood.* 109:4777–4785. http://dx.doi.org/10.1182/blood-2006-10-053280

Annex, B.H. 2013. Therapeutic angiogenesis for critical limb ischaemia. *Nat. Rev. Cardiol.* 10:387–396. http://dx.doi.org/10.1038/nrcardio.2013.70

Aranguren, X.L., X. Agirre, M. Beerens, G. Coppiello, M. Uriz, I. Vandersmissen, M. Benkheil, J. Panadero, N. Aguado, A. Pascual-Montano, et al. 2013. Unraveling a novel transcription factor code determining the human arterial-specific endothelial cell signature. *Blood.* 122:3982–3992. http://dx.doi.org/10.1182/blood-2013-02-483255

Arras, M., W.D. Ito, D. Scholz, B. Winkler, J. Schaper, and W. Schaper. 1998. Monocyte activation in angiogenesis and collateral growth in the rabbit hindlimb. *J. Clin. Invest.* 101:40–50. http://dx.doi.org/10.1172/JCI119877

Bach, A., Y. Lallemand, M.A. Nicola, C. Ramos, L. Mathis, M. Maufras, and B. Robert. 2003. *Msx1* is required for dorsal diencephalon patterning. *Development.* 130:4025–4036. http://dx.doi.org/10.1242/dev.00609

Buschmann, I., A. Pries, B. Styp-Rekowska, P. Hillmeister, L. Loufrani, D. Henrion, Y. Shi, A. Duelsner, I. Hoefer, N. Gatzke, et al. 2010. Pulsatile shear and Gja5 modulate arterial identity and remodeling events during flow-driven arteriogenesis. *Development.* 137:2187–2196. http://dx.doi.org/10.1242/dev.045351

Cai, W.J., M.B. Li, X. Wu, S. Wu, W. Zhu, D. Chen, M. Luo, I. Eitenmüller, A. Kampmann, J. Schaper, and W. Schaper. 2009. Activation of the integrins α5β1 and αvβ3 and focal adhesion kinase (FAK) during arteriogenesis. *Mol. Cell. Biochem.* 322:161–169. http://dx.doi.org/10.1007/s11010-008-9953-8

Cai, J., E. Pardali, G. Sánchez-Duffhues, and P. ten Dijke. 2012. BMP signaling in vascular diseases. *FEBS Lett.* 586:1993–2002. http://dx.doi.org/10.1016/j.febslet.2012.04.030

Chalothorn, D., and J.E. Faber. 2010. Strain-dependent variation in collateral circulatory function in mouse hindlimb. *Physiol. Genomics.* 42:469–479. http://dx.doi.org/10.1152/physiolgenomics.00070.2010

Chappell, D.C., S.E. Varner, R.M. Nerem, R.M. Medford, and R.W. Alexander. 1998. Oscillatory shear stress stimulates adhesion molecule expression in cultured human endothelium. *Circ. Res.* 82:532–539. http://dx.doi.org/10.1161/01.RES.82.5.532

Chen, Z., J. Rubin, and E. Tzima. 2010. Role of PECAM-1 in arteriogenesis and specification of preexisting collaterals. *Circ. Res.* 107:1355–1363. http://dx.doi.org/10.1161/CIRCRESAHA.110.229955

Cines, D.B., E.S. Pollak, C.A. Buck, J. Loscalzo, G.A. Zimmerman, R.P. McEver, J.S. Pober, T.M. Wick, B.A. Konkle, B.S. Schwartz, et al. 1998. Endothelial cells in physiology and in the pathophysiology of vascular disorders. *Blood.* 91:3527–3561 (PubMed).

Cross, E.E., R.T. Thomason, M. Martinez, C.R. Hopkins, C.C. Hong, and D.M. Bader. 2011. Application of small organic molecules reveals cooperative TGFβ and BMP regulation of mesothelial cell behaviors. *ACS Chem. Biol.* 6:952–961. http://dx.doi.org/10.1021/cb200205z

Dekker, R.J., S. van Soest, R.D. Fontijn, S. Salamanca, P.G. de Groot, E. VanBavel, H. Pannekoek, and A.J. Horrevoets. 2002. Prolonged fluid shear stress induces a distinct set of endothelial cell genes, most specifically lung Krüppel-like factor (KLF2). *Blood.* 100:1689–1698. http://dx.doi.org/10.1182/blood-2002-01-0046

dela Paz, N.G., and P.A. D'Amore. 2009. Arterial versus venous endothelial cells. *Cell Tissue Res.* 335:5–16. http://dx.doi.org/10.1007/s00441-008-0706-5

Derwall, M., R. Malhotra, C.S. Lai, Y. Beppu, E. Aikawa, J.S. Seehra, W.M. Zapol, K.D. Bloch, and P.B. Yu. 2012. Inhibition of bone morphogenetic protein signaling reduces vascular calcification and atherosclerosis. *Arterioscler. Thromb. Vasc. Biol.* 32:613–622. http://dx.doi.org/10.1161/ATVBAHA.111.242594

Duvall, C.L., W.R. Taylor, D. Weiss, and R.E. Guldberg. 2004. Quantitative microcomputed tomography analysis of collateral vessel development after ischemic injury. *Am. J. Physiol. Heart Circ. Physiol.* 287:H302–H310. http://dx.doi.org/10.1152/ajpheart.00928.2003

Eitenmüller, I., O. Volger, A. Kluge, K. Troidl, M. Barancik, W.J. Cai, M. Heil, F. Pipp, S. Fischer, A.J. Horrevoets, et al. 2006. The range of adaptation by collateral vessels after femoral artery occlusion. *Circ. Res.* 99:656–662. http://dx.doi.org/10.1161/01.RES.0000242560.77512.dd

Finnerty, J.R., M.E. Mazza, and P.A. Jezewski. 2009. Domain duplication, divergence, and loss events in vertebrate Msx paralogs reveal phylogenomically informed disease markers. *BMC Evol. Biol.* 9:18. http://dx.doi.org/10.1186/1471-2148-9-18

Fowkes, F.G., D. Rudan, I. Rudan, V. Aboyans, J.O. Denenberg, M.M. McDermott, P.E. Norman, U.K. Sampson, L.J. Williams, G.A. Mensah, and M.H. Criqui. 2013. Comparison of global estimates of prevalence and risk factors for peripheral artery disease in 2000 and 2010: a systematic review and analysis. *Lancet.* 382:1329–1340. http://dx.doi.org/10.1016/S0140-6736(13)61249-0

Fu, H., M. Ishii, Y. Gu, and R. Maxson. 2007. Conditional alleles of *Msx1* and *Msx2. Genesis.* 45:477–481. http://dx.doi.org/10.1002/dvg.20316

Goupille, O., C. Saint Cloment, M. Lopes, D. Montarras, and B. Robert. 2008. *Msx1* and *Msx2* are expressed in sub-populations of vascular smooth muscle cells. *Dev. Dyn.* 237:2187–2194. http://dx.doi.org/10.1002/dvdy.21619

Guzman, A., M. Zelman-Femiak, J.H. Boergermann, S. Paschkowsky, P.A. Kreuzaler, P. Fratzl, G.S. Harms, and P. Knaus. 2012. SMAD versus non-SMAD signaling is determined by lateral mobility of bone morphogenetic protein (BMP) receptors. *J. Biol. Chem.* 287:39492–39504. http://dx.doi.org/10.1074/jbc.M112.387639

Hao, J., J.N. Ho, J.A. Lewis, K.A. Karim, R.N. Daniels, P.R. Gentry, C.R. Hopkins, C.W. Lindsley, and C.C. Hong. 2010. *In vivo* structure-activity relationship study of dorsomorphin analogues identifies selective VEGF and BMP inhibitors. *ACS Chem. Biol.* 5:245–253. http://dx.doi.org/10.1021/cb9002865

Hayashi, K., S. Nakamura, W. Nishida, and K. Sobue. 2006. Bone morphogenetic protein-induced MSX1 and MSX2 inhibit myocardin-dependent smooth muscle gene transcription. *Mol. Cell. Biol.* 26:9456–9470. http://dx.doi.org/10.1128/MCB.00759-06

Helbing, T., R. Rothweiler, E. Ketterer, L. Goetz, J. Heinke, S. Grundmann, D. Duerschmied, C. Patterson, C. Bode, and M. Moser. 2011. BMP activity controlled by BMPER regulates the proinflammatory phenotype of endothelium. *Blood.* 118:5040–5049. http://dx.doi.org/10.1182/blood-2011-03-339762

Herzog, S., H. Sager, E. Khmelevski, A. Deylig, and W.D. Ito. 2002. Collateral arteries grow from preexisting anastomoses in the rat hindlimb. *Am. J. Physiol. Heart Circ. Physiol.* 283:H2012–H2020. http://dx.doi.org/10.1152/ajpheart.00257.2002

Holtwick, R., M. Gotthardt, B. Skryabin, M. Steinmetz, R. Potthast, B. Zetsche, R.E. Hammer, J. Herz, and M. Kuhn. 2002. Smooth muscle-selective deletion of guanylyl cyclase-A prevents the acute but not chronic effects of ANP on blood pressure. *Proc. Natl. Acad. Sci. USA.* 99:7142–7147. http://dx.doi.org/10.1073/pnas.102650499

Hu, J.S., L.T. Doan, D.S. Currle, M. Paff, J.Y. Rheem, R. Schreyer, B. Robert, and E.S. Monuki. 2008. Border formation in a Bmp gradient reduced to single dissociated cells. *Proc. Natl. Acad. Sci. USA.* 105:3398–3403. http://dx.doi.org/10.1073/pnas.0709100105

Ito, W.D., M. Arras, B. Winkler, D. Scholz, J. Schaper, and W. Schaper. 1997. Monocyte chemotactic protein-1 increases collateral and peripheral conductance after femoral artery occlusion. *Circ. Res.* 80:829–837. http://dx.doi.org/10.1161/01.RES.80.6.829

Jones, E.A., L. Yuan, C. Breant, R.J. Watts, and A. Eichmann. 2008. Separating genetic and hemodynamic defects in neuropilin 1 knockout embryos. *Development.* 135:2479–2488. http://dx.doi.org/10.1242/dev.014902

Kim, J.D., H. Kang, B. Larrivée, M.Y. Lee, M. Mettlen, S.L. Schmid, B.L. Roman, Y. Qyang, A. Eichmann, and S.W. Jin. 2012. Context-dependent proangiogenic function of bone morphogenetic protein signaling is mediated by disabled homolog 2. *Dev. Cell.* 23:441–448. http://dx.doi.org/10.1016/j.devcel.2012.07.007

Lallemand, Y., M.A. Nicola, C. Ramos, A. Bach, C.S. Clement, and B. Robert. 2005. Analysis of *Msx1*; *Msx2* double mutants reveals multiple roles for Msx genes in limb development. *Development.* 132:3003–3014. http://dx.doi.org/10.1242/dev.01877

le Noble, F., D. Moyon, L. Pardanaud, L. Yuan, V. Djonov, R. Matthijsen, C. Bréant, V. Fleury, and A. Eichmann. 2004. Flow regulates arteri-

al-venous differentiation in the chick embryo yolk sac. *Development.* 131:361–375. http://dx.doi.org/10.1242/dev.00929

Li, W., W. Shen, R. Gill, A. Corbly, B. Jones, R. Belagaje, Y. Zhang, S. Tang, Y. Chen, Y. Zhai, et al. 2006. High-resolution quantitative computed tomography demonstrating selective enhancement of medium-size collaterals by placental growth factor-1 in the mouse ischemic hindlimb. *Circulation.* 113:2445–2453. http://dx.doi.org/10.1161/CIRCULATIONAHA.105.586818

Liu, M., M.S. Kluger, A. D'Alessio, G. García-Cardeña, and J.S. Pober. 2008. Regulation of arterial-venous differences in tumor necrosis factor responsiveness of endothelial cells by anatomic context. *Am. J. Pathol.* 172:1088–1099. http://dx.doi.org/10.2353/ajpath.2008.070603

Lopes, M., O. Goupille, C. Saint Cloment, Y. Lallemand, A. Cumano, and B. Robert. 2011. Msx genes define a population of mural cell precursors required for head blood vessel maturation. *Development.* 138:3055–3066. http://dx.doi.org/10.1242/dev.063214

Lopes, M., O. Goupille, C. Saint Cloment, and B. Robert. 2012. *Msx1* is expressed in retina endothelial cells at artery branching sites. *Biol. Open.* 1:376–384. http://dx.doi.org/10.1242/bio.2012017

Mancini, M.L., A. Terzic, B.A. Conley, L.H. Oxburgh, T. Nicola, and C.P. Vary. 2009. Endoglin plays distinct roles in vascular smooth muscle cell recruitment and regulation of arteriovenous identity during angiogenesis. *Dev. Dyn.* 238:2479–2493. http://dx.doi.org/10.1002/dvdy.22066

Meier, P., S. Gloekler, R. Zbinden, S. Beckh, S.F. de Marchi, S. Zbinden, K. Wustmann, M. Billinger, R. Vogel, S. Cook, et al. 2007. Beneficial effect of recruitable collaterals: a 10-year follow-up study in patients with stable coronary artery disease undergoing quantitative collateral measurements. *Circulation.* 116:975–983. http://dx.doi.org/10.1161/CIRCULATIONAHA.107.703959

Moya, I.M., L. Umans, E. Maas, P.N. Pereira, K. Beets, A. Francis, W. Sents, E.J. Robertson, C.L. Mummery, D. Huylebroeck, and A. Zwijsen. 2012. Stalk cell phenotype depends on integration of Notch and Smad1/5 signaling cascades. *Dev. Cell.* 22:501–514. http://dx.doi.org/10.1016/j.devcel.2012.01.007

Moyon, D., L. Pardanaud, L. Yuan, C. Bréant, and A. Eichmann. 2001. Plasticity of endothelial cells during arterial-venous differentiation in the avian embryo. *Development.* 128:3359–3370 (PubMed).

Obi, S., K. Yamamoto, N. Shimizu, S. Kumagaya, T. Masumura, T. Sokabe, T. Asahara, and J. Ando. 2009. Fluid shear stress induces arterial differentiation of endothelial progenitor cells. *J. Appl. Physiol.* 106:203–211. http://dx.doi.org/10.1152/japplphysiol.00197.2008

Peñuelas, I., X.L. Aranguren, G. Abizanda, J.M. Martí-Climent, M. Uriz, M. Ecay, M. Collantes, G. Quincoces, J.A. Richter, and F. Prósper. 2007. (^{13})N-ammonia PET as a measurement of hindlimb perfusion in a mouse model of peripheral artery occlusive disease. *J. Nucl. Med.* 48:1216–1223. http://dx.doi.org/10.2967/jnumed.106.039180

Pi, X., P. Lockyer, L.A. Dyer, J.C. Schisler, B. Russell, S. Carey, D.T. Sweet, Z. Chen, E. Tzima, M.S. Willis, et al. 2012. Bmper inhibits endothelial expression of inflammatory adhesion molecules and protects against atherosclerosis. *Arterioscler. Thromb. Vasc. Biol.* 32:2214–2222. http://dx.doi.org/10.1161/ATVBAHA.112.252015

Pipp, F., S. Boehm, W.J. Cai, F. Adili, B. Ziegler, G. Karanovic, R. Ritter, J. Balzer, C. Scheler, W. Schaper, and T. Schmitz-Rixen. 2004. Elevated fluid shear stress enhances postocclusive collateral artery growth and gene expression in the pig hind limb. *Arterioscler. Thromb. Vasc. Biol.* 24:1664–1668. http://dx.doi.org/10.1161/01.ATV.0000138028.14390.e4

Rudini, N., A. Felici, C. Giampietro, M. Lampugnani, M. Corada, K. Swirsding, M. Garrè, S. Liebner, M. Letarte, P. ten Dijke, and E. Dejana. 2008. VE-cadherin is a critical endothelial regulator of TGF-β signalling. *EMBO J.* 27:993–1004. http://dx.doi.org/10.1038/emboj.2008.46

Sandelin, A., W. Alkema, P. Engström, W.W. Wasserman, and B. Lenhard. 2004. JASPAR: an open-access database for eukaryotic transcription factor binding profiles. *Nucleic Acids Res.* 32:D91–D94. http://dx.doi.org/10.1093/nar/gkh012

Satokata, I., and R. Maas. 1994. *Msx1* deficient mice exhibit cleft palate and abnormalities of craniofacial and tooth development. *Nat. Genet.* 6:348–356. http://dx.doi.org/10.1038/ng0494-348

Satokata, I., L. Ma, H. Ohshima, M. Bei, I. Woo, K. Nishizawa, T. Maeda, Y. Takano, M. Uchiyama, S. Heaney, et al. 2000. *Msx2* deficiency in mice causes pleiotropic defects in bone growth and ectodermal organ formation. *Nat. Genet.* 24:391–395. http://dx.doi.org/10.1038/74231

Scholz, D., W. Ito, I. Fleming, E. Deindl, A. Sauer, M. Wiesnet, R. Busse, J. Schaper, and W. Schaper. 2000. Ultrastructure and molecular histology of rabbit hind-limb collateral artery growth (arteriogenesis). *Virchows Arch.* 436:257–270. http://dx.doi.org/10.1007/s004280050039

Scholz, D., T. Ziegelhoeffer, A. Helisch, S. Wagner, C. Friedrich, T. Podzuweit, and W. Schaper. 2002. Contribution of arteriogenesis and angiogenesis to postocclusive hindlimb perfusion in mice. *J. Mol. Cell. Cardiol.* 34:775–787. http://dx.doi.org/10.1006/jmcc.2002.2013

Seghers, L., M.R. de Vries, E. Pardali, I.E. Hoefer, B.P. Hierck, P. ten Dijke, M.J. Goumans, and P.H. Quax. 2012. Shear induced collateral artery growth modulated by endoglin but not by ALK1. *J. Cell. Mol. Med.* 16:2440–2450. http://dx.doi.org/10.1111/j.1582-4934.2012.01561.x

Seki, T., J. Yun, and S.P. Oh. 2003. Arterial endothelium-specific activin receptor-like kinase 1 expression suggests its role in arterialization and vascular remodeling. *Circ. Res.* 93:682–689. http://dx.doi.org/10.1161/01.RES.0000095246.40391.3B

Somekawa, S., K. Imagawa, H. Hayashi, M. Sakabe, T. Ioka, G.E. Sato, K. Inada, T. Iwamoto, T. Mori, S. Uemura, et al. 2012. *Tmem100*, an ALK1 receptor signaling-dependent gene essential for arterial endothelium differentiation and vascular morphogenesis. *Proc. Natl. Acad. Sci. USA.* 109:12064–12069. http://dx.doi.org/10.1073/pnas.1207210109

Sorensen, L.K., B.S. Brooke, D.Y. Li, and L.D. Urness. 2003. Loss of distinct arterial and venous boundaries in mice lacking endoglin, a vascular-specific TGFbeta coreceptor. *Dev. Biol.* 261:235–250. http://dx.doi.org/10.1016/S0012-1606(03)00158-1

Sousa, V.H., G. Miyoshi, J. Hjerling-Leffler, T. Karayannis, and G. Fishell. 2009. Characterization of Nkx6-2-derived neocortical interneuron lineages. *Cereb. Cortex.* 19(Suppl 1):i1–i10. http://dx.doi.org/10.1093/cercor/bhp038

Sweet, D.T., Z. Chen, C.S. Givens, A.P. Owens III, M. Rojas, and E. Tzima. 2013. Endothelial Shc regulates arteriogenesis through dual control of arterial specification and inflammation via the notch and nuclear factor-κ-light-chain-enhancer of activated B-cell pathways. *Circ. Res.* 113:32–39. http://dx.doi.org/10.1161/CIRCRESAHA.113.301407

Tremblay, K.D., N.R. Dunn, and E.J. Robertson. 2001. Mouse embryos lacking Smad1 signals display defects in extra-embryonic tissues and germ cell formation. *Development.* 128:3609–3621 (PubMed).

Umans, L., L. Vermeire, A. Francis, H. Chang, D. Huylebroeck, and A. Zwijsen. 2003. Generation of a floxed allele of Smad5 for cre-mediated conditional knockout in the mouse. *Genesis.* 37:5–11. http://dx.doi.org/10.1002/gene.10219

Urness, L.D., L.K. Sorensen, and D.Y. Li. 2000. Arteriovenous malformations in mice lacking activin receptor-like kinase-1. *Nat. Genet.* 26:328–331. http://dx.doi.org/10.1038/81634

van der Meer, A.D., K. Vermeul, A.A. Poot, J. Feijen, and I. Vermes. 2010. A microfluidic wound-healing assay for quantifying endothelial cell migration. *Am. J. Physiol. Heart Circ. Physiol.* 298:H719–H725. http://dx.doi.org/10.1152/ajpheart.00933.2009

Wang, Y., M. Nakayama, M.E. Pitulescu, T.S. Schmidt, M.L. Bochenek, A. Sakakibara, S. Adams, A. Davy, U. Deutsch, U. Lüthi, et al. 2010. Ephrin-B2 controls VEGF-induced angiogenesis and lymphangiogenesis. *Nature.* 465:483–486. http://dx.doi.org/10.1038/nature09002

Wang, J., R.M. Kumar, V.J. Biggs, H. Lee, Y. Chen, M.H. Kagey, R.A. Young, and C. Abate-Shen. 2011. The Msx1 homeoprotein recruits polycomb to the nuclear periphery during development. *Dev. Cell.* 21:575–588. http://dx.doi.org/10.1016/j.devcel.2011.07.003

Weng, Q., Y. Chen, H. Wang, X. Xu, B. Yang, Q. He, W. Shou, Y. Chen, Y. Higashi, V. van den Berghe, et al. 2012. Dual-mode modulation of Smad signaling by Smad-interacting protein Sip1 is required for myelination in the central nervous system. *Neuron.* 73:713–728. http://dx.doi.org/10.1016/j.neuron.2011.12.021

Zhou, J., P.L. Lee, C.S. Tsai, C.I. Lee, T.L. Yang, H.S. Chuang, W.W. Lin, T.E. Lin, S.H. Lim, S.Y. Wei, et al. 2012. Force-specific activation of Smad1/5 regulates vascular endothelial cell cycle progression in response to disturbed flow. *Proc. Natl. Acad. Sci. USA.* 109:7770–7775. http://dx.doi.org/10.1073/pnas.1205476109

Zhou, J., P.L. Lee, C.I. Lee, S.Y. Wei, S.H. Lim, T.E. Lin, S. Chien, and J.J. Chiu. 2013. BMP receptor-integrin interaction mediates responses of vascular endothelial Smad1/5 and proliferation to disturbed flow. *J. Thromb. Haemost.* 11:741–755. http://dx.doi.org/10.1111/jth.12159